Analysis of cosmic radio noise absorption measured by the SGO riometer network

Pro Gradu
Mirjam Kellinsalmi
Degree Programme in Physics
University of Oulu
March 8, 2016

Oulun yliopisto **TIIVISTELMÄ OPINNÄYTETYÖSTÄ (liite FM-tutkielmaan)**
Luonnontieteellinen tiedekunta **Maisterintutkinnon kypsyysnäyte**

Fysiikan tutkinto-ohjelma **Pääaine** Fysiikka

Tekijä (Sukunimi ja etunimet)
Kellinsalmi Mirjam Elise

Tutkielman sivumäärä **70 + 2 liit.**

Työn nimi

Analysis of cosmic radio noise absorption measured by the SGO riometer network

Asiasanat: Riometer, Ionosphere, D-region, Absorption

Tiivistelmä

This thesis was made in collaboration with the Sodankylä Geophysical Observatory (SGO) and the Ionospheric Physics group in Oulu University. In my work I analysed data from the SGO riometer network. The data I used is from years 1997-2013, and seven stations located at different latitudes. The stations are located in Hornsund, Abisko, Ivalo, Sodankylä, Rovaniemi, Oulu and Jyväskylä. In the analysis I concentrated on comparing the effect of different quiet-day curve (QDC) methods to the statistics of absorption events. In my thesis I study the yearly number of absorption events and their diurnal variation in magnetic local time (MLT).

In my work I used absorption data calculated by two different QDC methods. The first method is based on automatic determination of the QDC and the second is based on manual determination. We decided to concentrate on using the data calculated by the automatic method, but I also compare our results to the manual data. In the beginning of this project I determined a simple method for finding absorption events from the riometer data. In collaboration with my supervisors and SGO staff we chose the criteria for an absorption event. I wrote a Matlab-script that was used to find the times and magnitudes of events from the data using the criteria. With this information I made the yearly and MLT-distributions to the automatic and manual data. We found a problem in the atomatic QDC method during the winter months of the maximum years of the solar cycle. We decided to manually remove the problematic periods. The automatic data set where the interfered periods are removed from forms the third data set used in this study, called the corrected automatic data.

The yearly distributions of absorption events in the corrected automatic and manual data set have similarities with the yearly average Kp index, which is the index of geomagnetic activity. The Kp maximum year, 2003, and the minimum year, 2009, are visible at most of the stations. Correlation with the yearly average sunspot number is less obvious, even though the 11-year cycle is visible in the absorption. Common features in the MLT-distribution are the morning maximum around 9 MLT and the evening minimum around 18 MLT. This is visible in the automatic and manual data to some extent at all stations. The MLT-distributions are slightly different each year, and during the minimum years of absorption it is significantly different. The morning maximum and evening minimum are not clearly visible. Most of our results are also visible in the uncorrected automatic data, excluding the years 2000-2003 and certain stations.

The data sets acquired from different QDC methods produced similar results, which gives credibility to them. There still are many interferences in the data, and it would require more work to remove them. The automatic QDC method should be refined so that it doesn't take into account data from times when the riometer has saturated. Our goal is to publish these results after some further analysis.

Muita tietoja

Päiväys: _____ / _____ 201_____ **Laatijan allekirjoitus**: _____

Oulun yliopisto **TIIVISTELMÄ OPINNÄYTETYÖSTÄ (liite FM-tutkielmaan)**
Luonnontieteellinen tiedekunta **Maisterintutkinnon kypsyysnäyte**

Fysiikan tutkinto-ohjelma **Pääaine** Fysiikka

Tekijä (Sukunimi ja etunimet)	**Tutkielman sivumäärä**
Kellinsalmi Mirjam Elise	**70 + 2 liit.**

Työn nimi

Analysis of cosmic radio noise absorption measured by the SGO riometer network

Asiasanat:
Riometri, Ionosfääri, D-kerros, Absorptio

Tiivistelmä

Tein Pro Gradu-tutkielmani yhteistyössä Sodankylän Geofysiikan Observatorion (SGO) ja Oulun yliopiston Ionosfäärifysiikan tutkimusryhmän kanssa. Työssäni analysoin SGO:n riometriverkoston dataa. Käyttämäni data on peräisin seitsemältä eri leveysasteilla sijaitsevalta asemalta vuosilta 1997-2013. Asemat sijaitsevat Hornsundissa, Abiskossa, Ivalossa, Sodankylässä, Rovaniemellä, Oulussa ja Jyväskylässä. Analyysissäni keskityin vertailemaan erilaisten hiljaisen päivän käyrän (Quiet Day Curve, QDC) määritysmenetelmien vaikutusta absorptioeventtien statistiikkaan. Tutkielmassani teen vertailua absorptioeventtien vuosittaisista määristä sekä niiden jakaumista magneettisen paikallisajan (Magnetic Local Time, MLT) funktiona.

Käytin työssäni kahdella eri menetelmällä määritettyä absorptiodataa. Ensimmäinen menetelmä perustuu QDC:n automaattiseen määritykseen ja toinen manuaaliseen määritykseen. Päätimme keskittyä käyttämään automaattisella menetelmällä määritettyä dataa, mutta työssäni vertailen tuloksia myös manuaaliseen dataan. Työni alussa kehitin yksinkertaisen tavan etsiä absorptioeventtejä riometridatasta. Yhdessä ohjaajieni ja SGO:n henkilökunnan avulla valitsimme kriteerit absorptioeventille. Kirjoittamani Matlab-ohjelma etsi datasta näillä kriteereillä absorptioeventtien ajankohdat sekä magnitudit. Näiden tietojen avulla tein vuosijakaumat ja MLT-jakaumat sekä manuaaliselle että automaattiselle datalle. Automaattisessa QDC-määritysessä ilmeni kuitenkin ongelmia auringonpilkkusyklin maksimivuosien talvikuukausina. Päätimme poistaa nämä ajanjaksot joilla ongelma ilmeni. Tämä automaattinen data josta häiriöitä oli poistettu muodosti kolmannen käyttämäni datasetin, korjatun automaattisen datan.

Absorptioeventtien vuosijakaumat automaattisessa ja manuaalisessa datassa noudattavat hyvin Kp-indeksiä, joka on geomagneettisen aktiivisuuden indeksi. Kp-indeksin maksimivuosi 2003 on havaittavissa monilla asemilla, kuin myös minimi vuonna 2009. Korrelaatio auringonpilkkuluvun vuosittaisen keskiarvon kanssa on vähemmän selkeä, vaikkakin 11 vuoden sykli on absorptiossa havaittavissa. MLT-jakaumissa yhdistävä piirre on aamumaksimi noin 9 MLT ja iltaminimi noin 18 MLT. Tämä on havaittavissa automaattisessa datassa ja manuaalisessa datassa jossain määrin kaikilla asemilla. MLT-jakauman muoto vaihtelee vuosittain, ja absorption minimivuosina se on hyvin erilainen, eivätkä aamumaksimi ja iltaminimi erotu selkeästi. Suuri osa saaduista tuloksista on myös nähtävissä korjaamattomassa datassa, lukuunottamatta vuosia 2000-2003 ja tiettyjä asemia.

Eri QDC-menetelmillä määritetyt datat, korjattu automaattinen ja manuaalinen data, tuottivat samanlaisia tuloksia ja kasvattavat tulosten luotettavuutta. Häiriöitä on kuitenkin edelleen datassa mukana, ja niiden tarkempi poistaminen vaatii vielä lisätyötä. QDC:n automaattista määritystä pitäisi myös kehittää niin, että se ei ottaisi huomioon ajanjaksoja jolloin riometri on saturoitunut. Tarkoituksemme on julkaista saamamme tulokset jatkoanalyysin jälkeen.

Muita tietoja

Päiväys: ____/ ____/ 201___ **Laatijan allekirjoitus**: _____

Acknowledgement

This project was done in collaboration with the Sodankylä Geophysical Observatory (SGO) and Ionospheric Physics group in Oulu University. Firstly, I want to thank my supervisors, Anita Aikio from the University of Oulu and Antti Kero from the Sodankylä Geophysical Observatory, for all the help, information and great ideas they have given.

Antti Kero and Tero Raita from SGO have been extremely helpful in providing the necessary data and helping with the technical aspects of the analysis. Tero Raita also did the tedious, but important, validation of the data. I also want to thank the rest of the SGO staff for support and genuine interest in the project, especially Thomas Ulich, Maxime Grandin, Alexandre Kozlovski, and the director of the observatory, Esa Turunen.

Contents

1 Introduction **7**

2 Theory **9**

2.1 The ionosphere and ionospheric phenomena 9

2.1.1 The ionosphere 9

2.1.2 The high-latitude ionosphere 10

2.1.3 D-region of the ionosphere 11

2.1.4 Radio wave absorption in the magnetoplasma of the D-region 11

2.2 The Sun and solar phenomena 13

2.2.1 Solar electromagnetic radiation 13

2.2.2 Solar eruptions 14

2.2.3 Sunspots 14

2.2.4 Solar wind 14

2.2.5 The Interplanetary Magnetic Field (IMF) 15

2.3 Earth's magnetosphere 16

2.3.1 Structure of the magnetosphere 16

2.3.2 The L-parameter 17

2.3.3 Van Allen particles and the trapping theory 18

2.3.4 Magnetic indices 20

3 The riometer **21**

3.1 The device 21

3.2 Finding the absorption 22

3.3 History and previous studies 22

3.3.1 Results from IRIS 24

4 Methods **29**

4.1 The SGO riometer network 29

4.2 Determining the quiet day curve (QDC) 30

4.2.1 Automatic method 30

4.2.2 Manual method 30
4.3 Defining an event 31
4.4 Corrections to the data 31

5 Results **35**
5.1 The data sets 35
5.2 Anomaly of 2000 - 2003 in the automatic data set 35
5.3 Yearly distributions 36
5.4 MLT distributions 45
5.4.1 Corrected automatic data 45
5.4.2 Manual data 55

6 Discussion **57**
6.1 Quality of the data 57
6.2 Effect of interferences 57
6.3 Yearly distributions and MLT distributions 60

7 Conclusions **65**

Appendices **71**

A Uncorrected automatic data **73**

B Manual data **81**

Chapter 1

Introduction

In this project we analysed riometer data from the Sodankylä Geophysical Observatory (SGO) riometer network from years 1997-2013. We searched for the times of occurring absorption events. The motivation behind it was that such a long time study with riometer data has not been done before. Also, because of the large amount of data, the results should be statistically reliable. The riometer measurements are from seven different observation sites, which are Hornsund, Abisko, Ivalo, Sodankylä, Rovaniemi, Oulu and Jyväskylä. This also gives a good coverage of different latitudes. Figure 1.1 shows the locations of the riometers in the SGO riometer network.

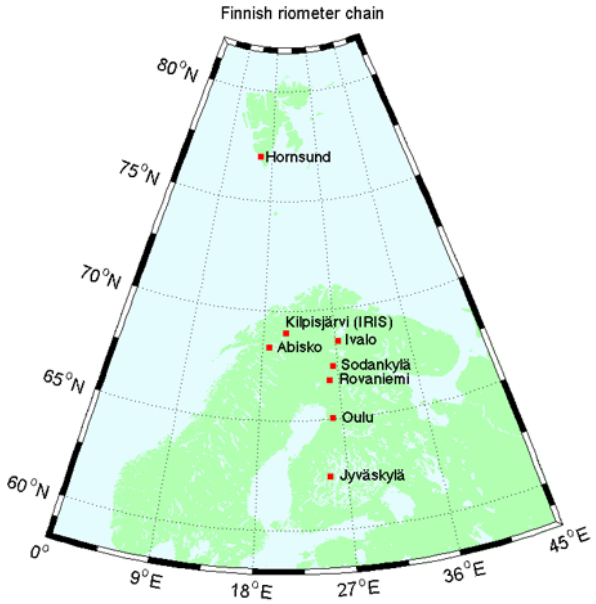

Figure 1.1: Locations of the riometers in the riometer network operated by SGO. Retrieved from SGO [2015].

The quality of the riometer data is not always good and external factors like military radio communications, temperature and snowfall can affect the measurements. First the data had to be checked for these interferences and in some cases ignore data from the affected days.

The goal was to find out during which magnetic local times (MLT), and at what stations, located at different latitudes, precipitation in the D-region can be observed. This is done by automatically going through the riometer absorption data and finding the events that meet certain criteria. Finally, I compare the results derived from two data sets, which use different quiet day curve methods.

Chapter 2

Theory

In this chapter I describe the main mechanisms how and why ionization is produced in Earth's atmosphere and especially in the high-latitude ionosphere. This forms the basis for understanding what the measured absorption is. The chapter is based on Hargreaves [1992], Hunsucker and Hargreaves [2003], Kavanagh [2002], Aikio and Nygrén [2016] and Mursula [2016].

2.1 The ionosphere and ionospheric phenomena

2.1.1 The ionosphere

The ionosphere is the ionized region of the atmosphere, comprising of neutrals, free electrons and positive ions, which create an ionized medium. The ionization is mainly caused by the extreme ultraviolet (EUV) and X-ray parts of the solar radiation spectrum.

There is a dynamic balance in the electron density. The rate of change is described by the continuity equation:

$$\frac{\partial N}{\partial t} = q - L - \nabla \cdot (N\mathbf{v}) \tag{2.1}$$

where N is the electron density, q is the production rate (per unit volume), L is the loss rate by recombination and $\mathbf{v}$ is the mean drift velocity of the electrons.

The ionosphere can be divided into different regions according to their ion chemistry. It is generally divided into three regions, the D-, E, and F-region. During daytime the F-region is divided into F_1 and F_2. During night time it consists of only one layer. There is also a sporadic E-layer, E_s, which is characterized by small,

thin clouds of intense ionization.

The different regions were discovered from radio reflections at different altitudes. They were later discovered to be from bulges in the continuous electron density profile (see figure 2.1). Listed below are some basic properties of the regions.

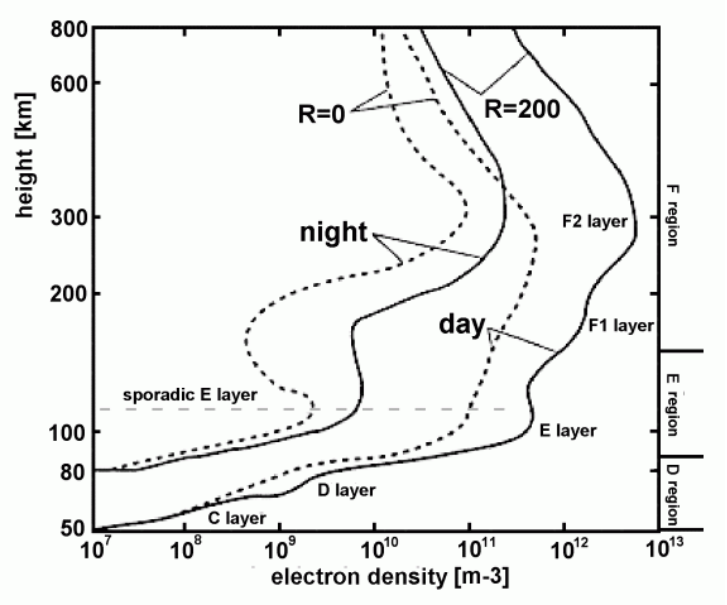

Figure 2.1: Day and night profiles of electron densities during solar minimum (R=0) and solar maximum time (R=200). Retrieved from INGV [2015].

- D-region: 60-90 km, $n_e = 10^8 - 10^{10}$ m^{-3}
- E-region: 90-150 km, $n_e = 10^{10} - 10^{11}$ m^{-3}
- F-region: 150-1000 km, $n_e = 10^{11} - 10^{12}$ m^{-3}

2.1.2 The high-latitude ionosphere

The ionosphere has different properties in different geomagnetic latitudes. It can be broadly divided into three regions which are the low-, mid- and high-latitude ionosphere.

In the high-latitude ionosphere the geomagnetic field is nearly vertical. The magnetic field-lines connect to the outer part of the magnetosphere, which is strongly affected by the solar wind. The region is also more accessible to energetic particle precipitation from the magnetosphere which can cause additional ionization. The auroral oval occurs in the high-latitude region and there are also substorms during

which energetic electrons arrive in the ionosphere causing a great increase in the ionization rate [Hunsucker and Hargreaves, 2003].

2.1.3 D-region of the ionosphere

There is a lot of day-night variation in the D-region and solar events can also have a significant effect on it. The D-region reduces greatly after sunset due to the reduced solar ionization. However, energetic particle precipitation can produce ionization in the region at all times.

The atmospheric neutral density in the D-region is about 10^6 times higher than in the F-region and collisions are dominant. Most abundant molecules are N_2, O_2, NO and their ions (N_2^+, O_2^+, NO^+). There are also negative ions (O_2^-) in the lower D-region. Important ionization sources in the region are:

- Lyman-α line (121.5 nm), which ionizes nitric oxide NO.
- EUV radiation (between 102.7-111.8 nm) ionizes excited oxygen molecules O_2.
- Hard X-rays (between 0.2-0.8 nm) ionize all constituents.
- Galactic cosmic rays ionize all constituents.
- Occasionally also relativistic electrons and protons can cause ionization.

2.1.4 Radio wave absorption in the magnetoplasma of the D-region

Magnetoplasma

Earth's upper atmosphere is partly ionized and the geomagnetic field permeates the ionized gas. Magnetoplasma is the combination of a magnetic field and ionized gas. In the magnetic field electrons are forced into circular motion by the Lorentz force

$$\mathbf{F} = -e \cdot \mathbf{v} \times \mathbf{B} \ , \tag{2.2}$$

where $\mathbf{B}$ is the magnetic flux density, e is the electron charge and $\mathbf{v}$ is the velocity vector. The Lorentz force provides acceleration v^2/r_B, where r_B is the radius of the circle. So the *gyroradius* is

$$r_B = \frac{m_e v}{Be} \ , \tag{2.3}$$

where m_e is the electron mass. The rate of the gyration is called *gyrofrequency*. The time taken by one revolution is $T = 2\pi r_B/v$, so the *angular gyrofrequency* [rad/s] is

$$\omega_B = \frac{2\pi}{T} = \frac{Be}{m_e} , \tag{2.4}$$

The *plasma frequency* describes the natural oscillation frequency for electrostatic perturbations in plasma. Angular plasma frequency for electrons ω_N is defined as

$$\omega_N = \sqrt{\frac{Ne^2}{\epsilon_0 m_e}} , \tag{2.5}$$

where N is the electron number density measured in m^{-3} and ϵ_0 is vacuum permittivity.

Absorption of radio waves in the D-region

This section is based on Hargreaves [1992], pp. 25-26, 65. The *magnetoionic theory* describes the propagation of radio waves in uniform magnetoplasma. Radio waves are attenuated in the D-region because of absorption. The formula for the refractive index of an ionized medium is called the *Appleton-Hartree equation*

$$n^2 = 1 - \frac{X}{1 - iZ - (\frac{Y_T^2}{2(1-X-iZ)}) \pm (\frac{Y_T^4}{4(1-X-iZ)^2} + Y_L^2)^{\frac{1}{2}}} \tag{2.6}$$

where $n = \mu - i\chi$ is a complex refractive index, and X, Y and Z are:

$$\begin{cases} X = \omega_N^2/\omega^2, \\ Y = \omega_B/\omega, \\ Y_L = \omega_L/\omega, \\ Y_T = \omega_T/\omega, \\ Z = \nu/\omega \end{cases}$$

Here ν is the electron collision frequency and ω is the angular wave frequency, and ω_N and ω_B are the angular plasma frequency and the electron gyrofrequency which are defined by equations 2.3 and 2.5 respectively. ω_L and ω_T are the longitudinal and transverse components of ω_B with respect to the direction of propagation. If θ is the angle between the geomagnetic field and the direction of propagation

$$\begin{cases} \omega_L = \omega_B \cos\theta \\ \omega_T = \omega_B \sin\theta. \end{cases} \tag{2.7}$$

The imaginary term of the refractive index n describes the attenuation of the electromagnetic wave. If collisions are taken into account ($Z \neq 0$) but the effects of the magnetic field are small, the terms containing Y_T and Y_L can be ignored. Then the formula for the refractive index becomes

$$n^2 = 1 - \frac{X}{iZ} = 1 - \frac{\omega_N^2}{\omega(\omega - i\nu)} \ . \tag{2.8}$$

The absorption coefficient κ (in units of nepers/m) is given by

$$\kappa = \frac{\omega\chi}{c} = \frac{\omega}{c} \cdot \frac{1}{2\mu} \cdot \frac{XZ}{1+Z^2} = \frac{e^2}{2\epsilon_0 m_e c} \cdot \frac{1}{\mu} \cdot \frac{N\nu}{\omega^2 + \nu^2} \ , \tag{2.9}$$

where c is the speed of light in a vacuum. A special case that applies to the lower ionosphere is the *non-deviative absorption*, $\mu = 1$, because the velocity of the wave is not altered and so there is no bending. In that case,

$$\kappa = \frac{e^2}{2\epsilon_0 m_e c} \cdot \frac{N\nu}{\omega^2 + \nu^2} \ . \tag{2.10}$$

Putting in the values of the physical constants and using the relation
1 neper $\approx$ 8.686 dB gives the formula of absorption in decibels [dB] in the lower ionosphere

$$A = 4.5 \cdot 10^{-5} \int \frac{\mathrm{N}\nu}{\omega^2 + \nu^2} dz \ , \tag{2.11}$$

where the integration is made along path dz in the direction of wave propagation. The absorption discussed in this thesis is, in accordance with equation 2.11, measurements of collisional plasma electron densities in the D-region.

2.2 The Sun and solar phenomena

2.2.1 Solar electromagnetic radiation

The Sun radiates electromagnetic radiation in a broad spectrum which can be described with the black body radiation at a temperature $T = 5780$ K. The most significant parts of the spectrum in the interaction with the Earth's atmosphere are the ultraviolet and X-ray frequencies. The intensity of radiation in these wavelengths follows a periodicity of eleven years, called the solar cycle. The emissions in these wavelengths vary a lot according to solar activity and can be greatly enhanced during solar flare events.

2.2.2 Solar eruptions

A solar flare happens when a large amount of magnetic energy is suddenly released. A great amount of highly energetic particles and electromagnetic radiation is released. A flare is seen as a sudden brightening in the photosphere and can be followed by a coronal mass ejection (CME). During a CME material from the Sun is ejected and released into the solar wind. Solar flares are the source of sporadic particle and electromagnetic emissions that affect the Earth's upper atmosphere. Flares can cause a proton event on Earth when a flux of energetic (1-1000 MeV) protons is produced. When the energetic protons enter the atmosphere, they lose energy in collisions between the neutral molecules and produce ionization. Protons with initial energies ranging 1-100 MeV can affect the ionosphere at the altitude of 35-90 km (Hunsucker and Hargreaves [2003], pp. 109, 400).

2.2.3 Sunspots

Sunspots are visibly darker areas on the surface of the Sun. They are produced by strong magnetic flux densities, and thus are an indicator of the magnetic activity of the Sun. The number of sunspots also follows an 11-year cycle and is called the sunspot cycle.

There are different ways for computing the sunspot number. The most commonly used is the international sunspot number. It is computed by calculating the number of individual sunspots, s, and the sunspot groups, g. The sunspot number R is then given by:

$$R = k(10g + s), \tag{2.12}$$

where k is the observatory factor that varies with location and instrumentation. In our study we compared the yearly average international sunspot number to the yearly number of absorption events (see Chapter 5.3).

2.2.4 Solar wind

The outer atmosphere of the Sun is radially expanded to the interplanetary space and is known as the solar wind. The solar wind is plasma, comprising mainly of electrons and protons that are energetic enough to escape the Sun's gravity. The flux of particles with energy exceeding 25 eV is between $2 - 7 \cdot 10^{12}$ $\mathrm{m^{-2}s^{-1}}$ (Hargreaves [1992], p. 144). Most of the ions are protons (H^+), but there are also α-particles,

usually amounting to about 5 %. At 1 AU the solar wind typically has velocity between 300-700 km/s [Gosling et al., 1976]. The variability in density and speed of the solar wind is large during the solar cycle. Solar phenomena, solar flares and high speed streams (HSS), can greatly affect the solar wind parameters. The effect of solar wind velocity on ionospheric absorption is discussed in Chapter 3.3.

2.2.5 The Interplanetary Magnetic Field (IMF)

The solar wind carries a weak magnetic field, varying from 1 to 37 nT (Zolesi and Cander [2013], p. 20). The field is frozen into the plasma. This happens because of the large electrical conductivity of the plasma, which makes relative motion between the plasma and the magnetic field virtually impossible. Solar rotation gives the field a spiral form (Archimedian spiral or Parker spiral). At the orbit of Earth the field lines are approximately 45^o to the radial direction, so the east-west components of the IMF are about equal in magnitude. The IMF can be oriented either inward or outward, and there can be more than two sectors. The neutral current sheet separates the oppositely directed fields. Because the solar magnetic dipole is tilted from the rotation axis, we periodically see the different sectors. In the *ballerina model* these undulations in the current sheet are visualized as a pirouetting ballerina's skirt, see figure 2.2. The direction of the IMF near Earth can affect radio wave absorption in the D-region [Kavanagh, 2002]. This is discussed more in Chapter 3.3.

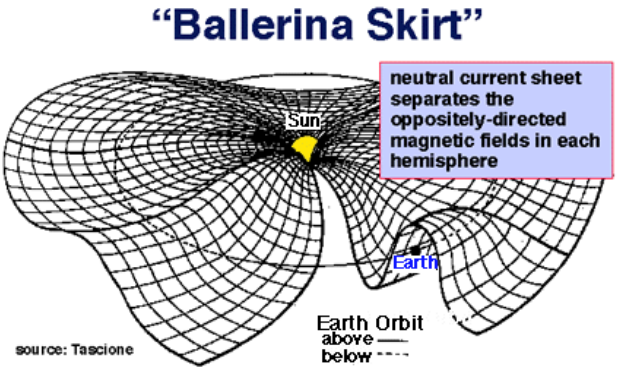

Figure 2.2: Visualization of the undulations in the neutral current sheet, also known as the ballerina skirt model. Retrieved from UCAR [2000].

2.3 Earth's magnetosphere

2.3.1 Structure of the magnetosphere

Figure 2.3 shows the shape and different regions of the Earth's magnetosphere. The Earth has a magnetic field which forms a barrier between the solar wind and the planet. The boundary between the geomagnetic field and incident solar wind is called the magnetopause. When the system is in an equilibrium, the pressure of the solar wind equals the pressure of the magnetic field.

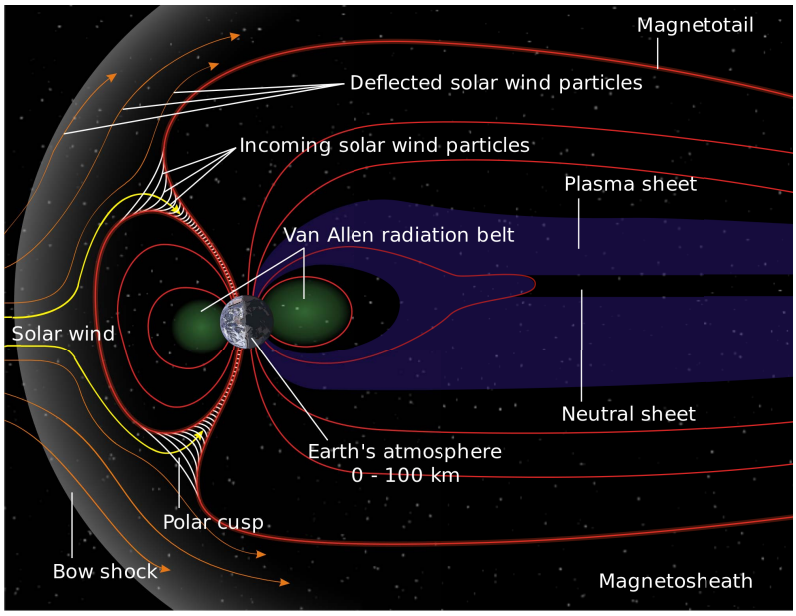

Figure 2.3: A schematic figure of the different regions of Earth's magnetosphere. Retrieved from NASA [2007].

The solar wind flows along the boundary of the magnetosphere and causes pressure on the day side magnetosphere and the field becomes compressed. The magnetosphere is stretched into a long tail in the night side. There is a central plane where the field direction is reversed. This is called the neutral sheet.

In the inner magnetosphere is the plasmasphere consisting of electrons, photons and some heavy ions. It is a dense and cold region, bounded by a sharp change in density that is called the plasmapause.

The plasma sheet is associated with the neutral sheet in the magnetotail. The particles in plasma sheet are energized within the magnetotail and are important in the behaviour of the high-latitude ionosphere. The inner edge of the plasma sheet

supports the ring current. It flows in the magnetosphere during magnetic storms.

2.3.2 The L-parameter

The magnetic field lines inside the magnetosphere are described using the L shell parameter [McIlwain, 1961]. The parameter is equal to the distance in Earth radii R_E from the center of the Earth at which the magnetic field line crosses the magnetic equator.

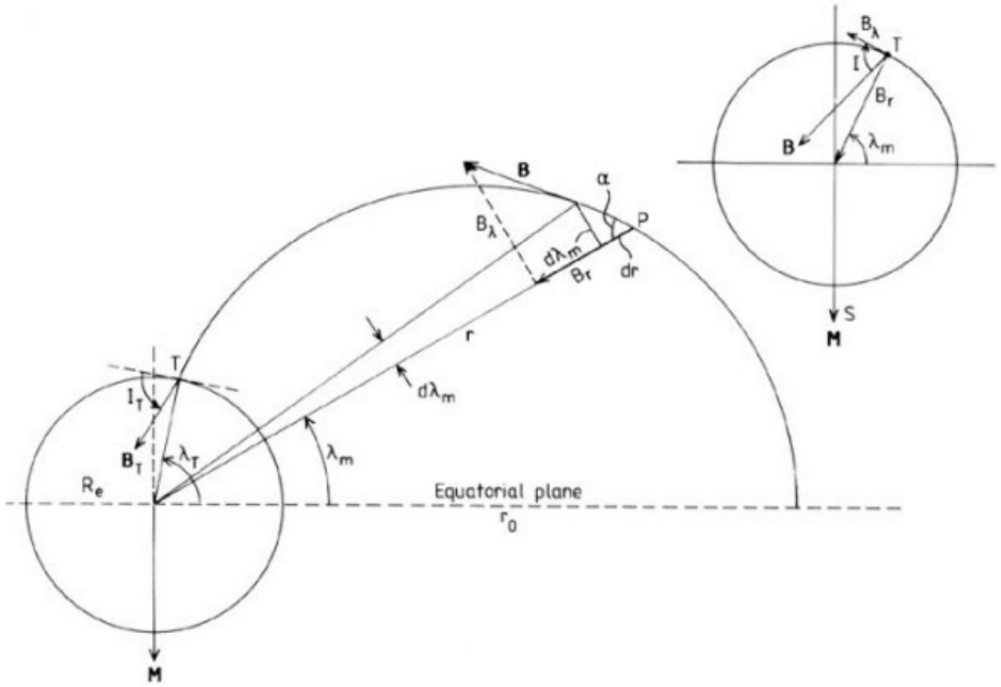

Figure 2.4: Field line in a dipole field [Mursula, 2015]. The symbol λ_m in the figure corresponds to λ in the text, and λ_T corresponds to λ_0.

The following description is based on Mursula [2015]. The equation of a magnetic dipole field **B** can be expressed as

$$\mathbf{B}(r,\lambda) = B_r(r,\lambda)\mathbf{e}_r + B_\lambda(r,\lambda)\mathbf{e}_\lambda = H_1(\frac{R_E}{r})^3(-2\sin\lambda\mathbf{e}_r + \cos\lambda\mathbf{e}_\lambda) \ , \qquad (2.13)$$

where R_E is the radius of the Earth, r is the radial distance from Earth's center to the field line and λ is the angle between **r** and the equatorial plane. They are shown in figure 2.4. The angle α between the magnetic field vector and **r** can be derived from a local magnetic field line tangent

$$\tan\alpha = \frac{B_\lambda}{B_r} = -\frac{\cos\lambda}{2\sin\lambda} \ , \tag{2.14}$$

where B_r and B_λ are obtained from equation 2.13 and they are shown in figure 2.4. The angle α can also be derived from

$$\tan\alpha = \frac{rd\lambda}{dr} \ . \tag{2.15}$$

$d\lambda$ and dr are also shown in figure 2.4. Combined, these give the equation

$$\frac{dr}{r} = -2\frac{\sin\lambda}{\cos\lambda}d\lambda \ . \tag{2.16}$$

Integration gives

$$\ln r = 2\ln\cos\lambda + C' \Leftrightarrow \ r = C\cos^2\lambda \ . \tag{2.17}$$

At the magnetic equator $\lambda = 0$ and $r(0) = r_0 = C$. This yields the equation for the magnetic field line in a dipole field

$$r = r_0\cos^2\lambda \ . \tag{2.18}$$

This can be written with the L-parameter when r_0 is expressed as $r_0 = L \cdot R_E$

$$r = L \cdot R_E\cos^2\lambda \ . \tag{2.19}$$

The field line reaches Earth's surface at a latitude λ_0, substituting $r = R_E$ to the equation 2.19, L can be solved

$$L = \frac{1}{\cos^2\lambda_0} \ . \tag{2.20}$$

λ_0 is known as the invariant latitude because it is the same for the entire field line. The L-values for each SGO riometer station are shown in Table 4.1.

2.3.3 Van Allen particles and the trapping theory

The regions of trapped energetic particles in the magnetosphere are located in dipolar magnetic field lines. They are called the Van Allen belts, or the radiation belts. The trapped particles can precipitate into the ionosphere and cause ionization. The trapping is due to the interaction between a static magnetic field and a moving electric charge.

If a particle in the magnetosphere has velocity $v_\parallel$ parallel to the magnetic field and $v_\perp$ perpendicular to it, its trajectory is a spiral and the gyroradius r_B is defined in section 2.1 equation 2.3. If no work is done on the particle the magnetic flux through its orbit Φ_m is constant. This means that

$$\Phi_m = B \cdot \pi r_B^2 = \frac{2\pi m W_\perp}{e^2 B} = \text{constant}, \tag{2.21}$$

where $W_\perp$ is the perpendicular kinetic energy, $E_\perp = mv_\perp^2/2$. Equation 2.21 implies that $W_\perp/B$ is constant, which is the magnetic moment of the current loop created by the gyrating particle

$$\mu = \text{current} \times \text{area} = \frac{ev_\perp}{2\pi r_B} \cdot \pi r_B^2 = mv_\perp^2/2B = W_\perp/B \ . \tag{2.22}$$

This is called the *first adiabatic invariant* of charged particle motion in a magnetic field: the magnetic moment is constant. This is true in cases where the magnetic field doesn't change much during a gyration period.

The pitch angle α is the angle between the velocity vector of the particle and the magnetic field line. The perpendicular velocity $v_\perp = v \sin\alpha$. Equation 2.22 can be written as

$$W_\perp/B = W \sin^2\alpha/B = \text{constant}. \tag{2.23}$$

Because the total kinetic energy W is constant we get

$$\sin^2\alpha \propto \text{B}. \tag{2.24}$$

As the particle moves from the magnetospheric equator towards the ionosphere, it faces an increasing magnetic field and the pitch angle increases. Eventually, when $\alpha = 90^o$, the forward motion of the particle stops, and it is reflected back towards the equator. This is called the mirror point. Figure 2.5 describes the motion of charged particles in the geomagnetic field.

If the particle encounters the atmosphere before reaching the mirror point it will be lost there. The equatorial pitch angles of the particles that will be lost at the next bounce define the loss cone. This is the basic mechanism of particle precipitation into the atmosphere. The pitch angle of a particle can be changed e.g. through transverse resonance with a very low frequency (VLF) wave [Hargreaves, 1992]. When a gyrating electron feeds energy into a VLF wave its velocity transverse to the magnetic field is reduced, but the parallel velocity remains unchanged. VLF *whistlers* can propagate between the hemispheres along the geomagnetic field. Whistler mode refers to propagation of a radio wave with a frequency below the plasma frequency

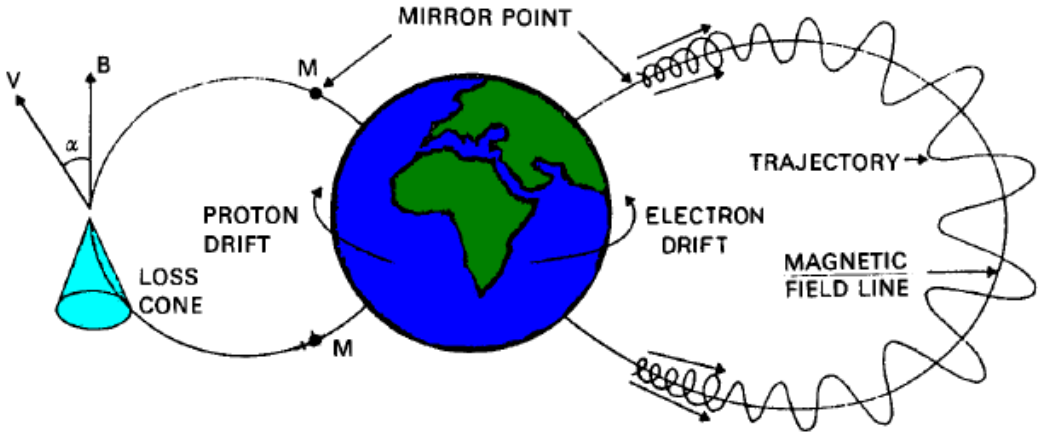

Figure 2.5: The trajectory of charged particles along the geomagnetic field-line. The mirror points and the loss cone are also shown. Copy from Kavanagh [2002], originally by J. Lemaire [1982].

of the medium. Chorus emissions are intense whistler-mode waves which are excited in the low-density region outside plasmapause by the injection of plasmasheet electrons into the inner magnetosphere during enhanced storm-time convection [Thorne et al., 2013].

2.3.4 Magnetic indices

Several different indices are regularly calculated from magnetic records. They describe the level of magnetic disturbances in the Earth's magnetic field. Most widely used are the K_p and A_p indices. The K index describes disturbances in the horizontal component of the Earth's magnetic field. The planetary K_p index is a weighted average of the K-index from several different stations. K_p ranges from 0 to 9 and is quasi-logarithmic. A_p is the linearly scaled equivalent of K_p, and it ranges from 0 to 400. In our study we compared the yearly average K_p-index to yearly number of absorption events (see Chapter 5.3).

Chapter 3

The riometer

3.1 The device

A riometer (Relative Ionospheric Opacity Meter, Extra-Terrestrial Electromagnetic Radiation) is a passive radio antenna which typically works in the frequency range of 30-50 MHz. SGO uses wide-beam riometers that measure a 60°-wide beam-shaped area above it. There are also phased narrow-beam riometers, e.g. the imaging riometer KAIRA in Kilpisjärvi [McKay-Bukowski et al., 2015]. Table 4.1 shows the co-ordinates and L-values of the SGO riometer stations.

A riometer measures the opacity of the D-region of the ionosphere to radio noise coming from natural astronomical sources such as the center of the Milky Way, the Sun, Jupiter, Cassiopeia A, and many lesser galactic sources. Radio communications on Earth can also cause interferences in the measurements.

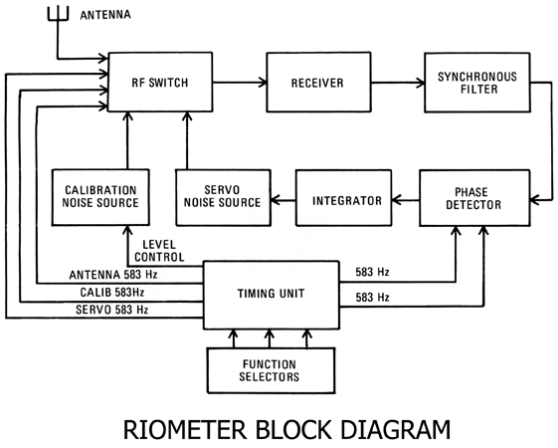

Figure 3.1: Block diagram of a La Jolla riometer [LaJolla, 2010].

The device consists of an antenna and a self-balancing receiving system where a

local noise source is continuously made equal to the noise power from the antenna [Little and Leinbach, 1959]. This makes it possible to monitor the cosmic radio emissions continuously. Figure 3.1 shows a block diagram of a La Jolla riometer.

3.2 Finding the absorption

Since the galactic radio flux is constant over long periods of time, changes of apparent intensity from one day to another at the same sidereal time represent corresponding changes in the ionospheric absorption. Finding the absorption requires the determination of a quiet day curve (QDC), which is an estimate of the signal level in the absence of additional absorption. This can, for example, be done by superimposing measurements over a period of time (several days) and taking a line along the top of the distribution [Hunsucker and Hargreaves, 2003]. The methods SGO uses for defining the QDC are explained in Chapter 4. The absorption is seen as a deviation from the QDC, as the received signal drops. The absorption A in decibels is given by

$$A = 10 \cdot \log \frac{P_{QD}}{P} \ , \tag{3.1}$$

where P_{QD} is the quiet-day power and P is the measured power.

3.3 History and previous studies

Auroral radio absorption was first discovered by Appleton, Naismith and Builder during the International Polar Year in 1932-1933 [Appleton et al., 1933]. By the International Geophysical Year of 1957-1958, several studies had been made, mainly by radio reflection methods, which established a clear distinction between the high-latitude absorption and the absorption at mid- and low-latitudes. High-latitude absorption was discovered to be dominated by geophysical disturbances and auroral activity, e.g. Agy [1954], Heppner et al. [1952] and Wells [1947].

The riometer technique is based on the cosmic noise method. It was developed at the Geophysical Institute of the University of Alaska [Little and Leinbach, 1959] and was found to be very useful in measuring the D-region absorption and ionospheric disturbances. Two types of of high-latitude absorption were found as described by Reid and C. [1959] and Obayashi and Hakura [1960]: polar cap absorption (PCA) and auroral absorption (AA), which is due to the entry of auroral electrons. PCA was first identified by Bailey [1957], as the absorption that is due to the abnormal

ionization produced by the incidence of solar protons after an intense solar flare. Both can produce over 10 dB of absorption on a 30 MHz riometer, but PCA tends to be smooth and last for days and AA is more irregular. A third type is sudden commencement absorption (SCA), which is due to sudden commencement magnetic storms [Ortner et al., 1962].

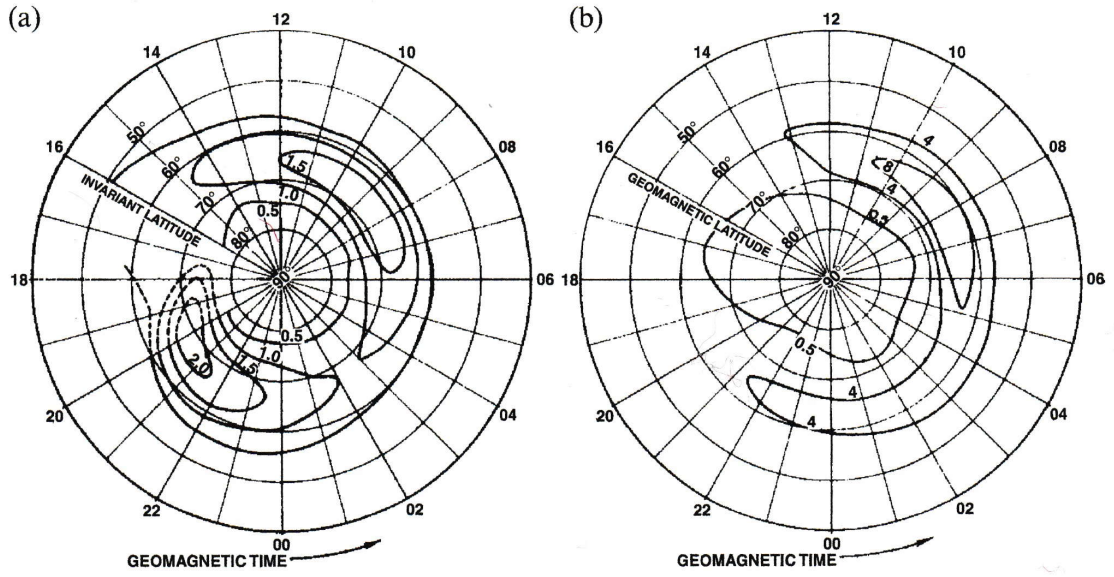

Figure 3.2: (a) shows the median intensity of AA at 30 MHz [Hargreaves and Cowley, 1967] and (b) the percentage occurrence of 30-MHz absorption exceeding 1 dB [Hartz et al., 1963]. Copy from the book by Hargreaves [1992].

Complex time and space variations are observed in the auroral absorption. The activity is concentrated on geomagnetically preferred zones, e.g. Hargreaves and Cowley [1967] and Hartz et al. [1963]. Figure 3.2 (a) shows the distribution of the median intensity of auroral absorption at 30 MHz in MLT and latitude, and (b) the percentage of the time 1 dB absorption is exceeded. The positions of the zones vary and the level of activity changes with solar activity. Cycles of one month and 11 years are prominent. Also seasonal variations are seen, which probably are related to the changes in the shape of the magnetosphere, as the dipole axis tilts with respect to solar wind. Seasonal variation at the south pole was studied by Hargreaves [2007].

The diurnal variation in the intensity of absorption is also visible in the figure 3.2. Usually two maximums can be seen, one before magnetic midnight and another before magnetic noon [Hartz et al., 1963], but the times of the maxima vary with latitude. Events during the day tend to last longer than night-time events. The diurnal patterns change with the planetary level of magnetic activity [Hargreaves

and Cowley, 1967].

A distinguishing feature of auroral absorption is its temporal structure. Many different features can be seen in the absorption graphs, for example spike events, where the absorption rises sharply and lasts only for a few minutes, and slowly varying events, which can last for hours and have a smooth shape. Auroral absorption is stronger and more frequent when geomagnetic activity is high. The correlation with solar activity indices, like the sunspot number, is complicated [Hargreaves et al., 1987]. In some solar cycles magnetic activity doesn't follow the sunspot number and in these cases the AA follows the magnetic activity (A_p) rather than the sunspot number. A thorough summary of the results from the first decade of riometry is given by Hargreaves [1969].

3.3.1 Results from IRIS

In his doctoral thesis Kavanagh [2002] used riometer data from the imaging riometer for ionospheric studies, IRIS, located in Kilpisjärvi (L=6.2), Finland [IRIS, 2015]. His study included data from six years, 1995 - 2001. Figure 3.3 shows the mean absorption for 10 minute intervals each year by magnetic local time from the IRIS station, which uses a 38.2 MHz frequency. The absorption is more intense in 1995 and 1998 - 2000 between the magnetic local times 06 - 13. A clear minimum takes place between 17-20 MLT during all years.

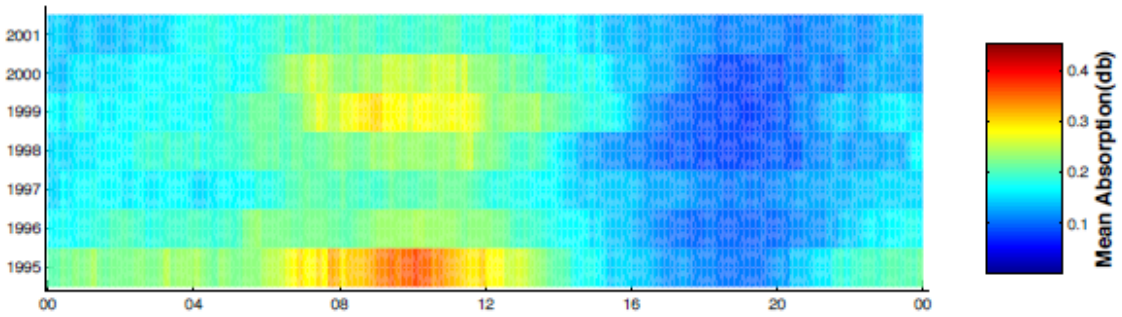

Figure 3.3: Mean absorption for 10-minute intervals by magnetic local time for years 1995 - 2001 by IRIS, Kavanagh [2002], p. 153.

Kavanagh also studied the mean absorption during each season by MLT and in different magnetic latitudes ranging from 64.97° to 66.86°. The results are shown in figure 3.4. The mean absorption is least intense during summer, and highest during spring and autumn between magnetic latitudes $65.5° - 66.5°$.

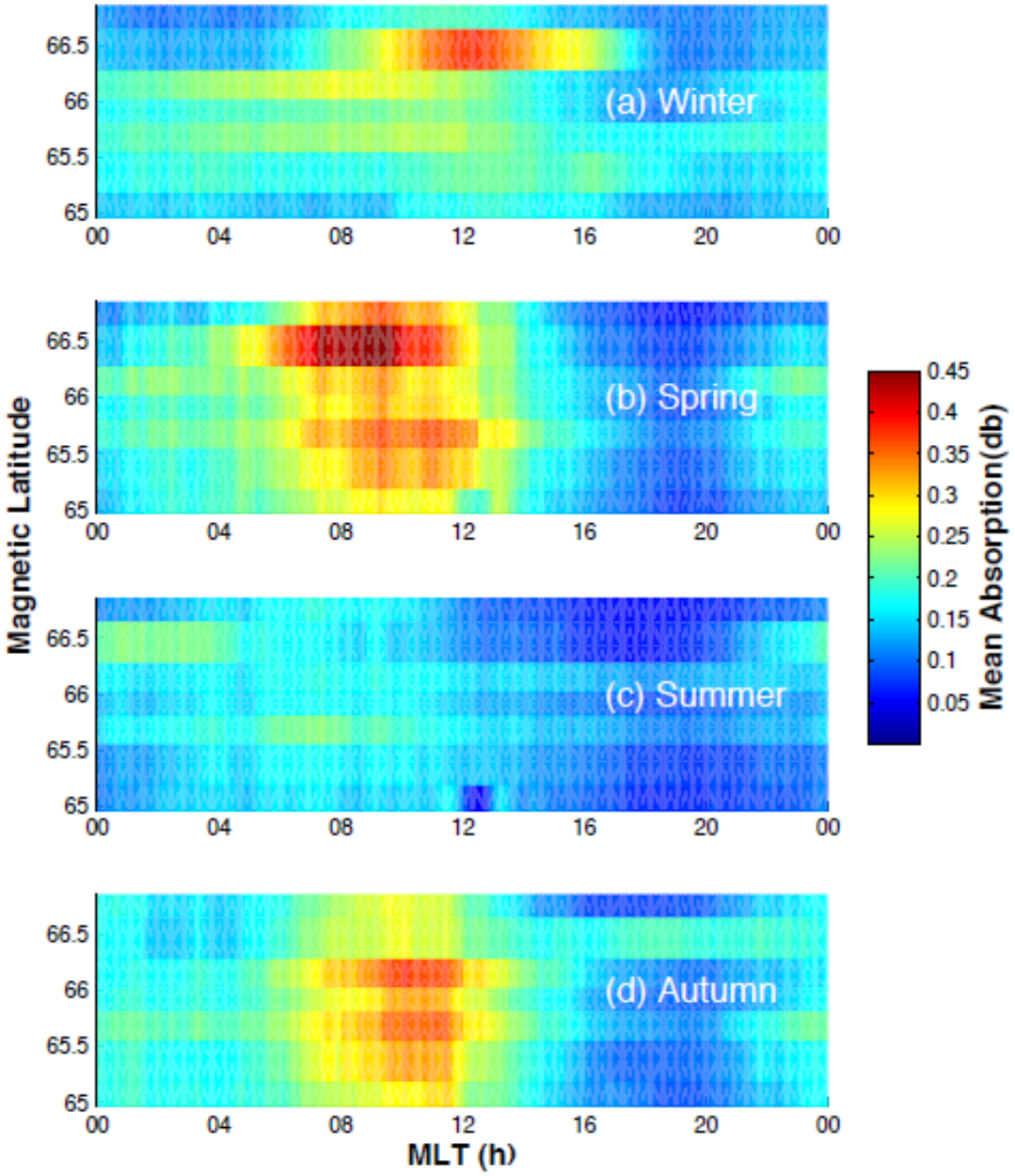

Figure 3.4: Mean absorption for each season by magnetic latitude from IRIS measurements in Kilpisjärvi, 1995 - 2001. Winter (December to February), Spring (March to May), Summer (June to August), Autumn (September to November) [Kavanagh, 2002].

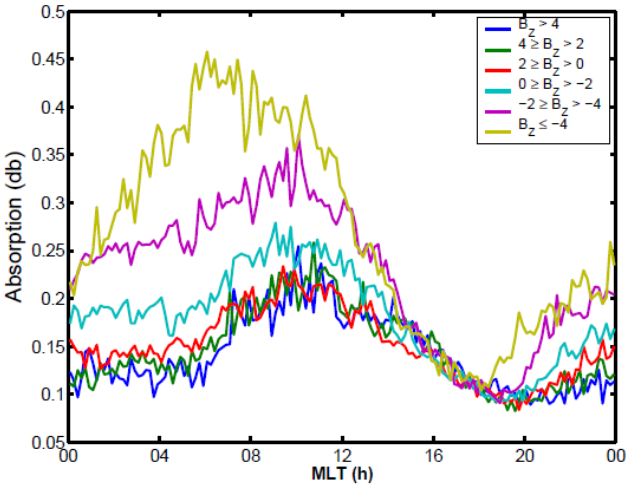

Figure 3.5: Ten-minute averaged absorption binned with IMF Bz. Increasingly negative Bz increases absorption in the early morning and midnight sectors [Kavanagh et al., 2004].

Kavanagh et al. [2004] studied the effects of the IMF, solar wind speed and the K_p index on absorption based on data from IRIS. Figure 3.5 shows the absorption with the IMF Bz component. It shows ten-minute averaged absorption binned with the Bz. A northward IMF does not affect absorption but negative Bz values tend to increase absorption in the morning and night. The least intense absorption values are measured at approximately 19 MLT, and the highest values at 05 MLT, when $B_z \leq -4$, and at 10 MLT when $B_z > 4$.

Absorption and the K_p index is shown in figure 3.6. The correlation is strongest between 03-12 MLT, and weakest in 18-21 MLT. Absorption and the solar wind velocity are shown in figure 3.7. The solar wind speed correlates with the absorption, most clearly between 03 and 12 MLT. The correlation is least clear between 15 - 21 MLT.

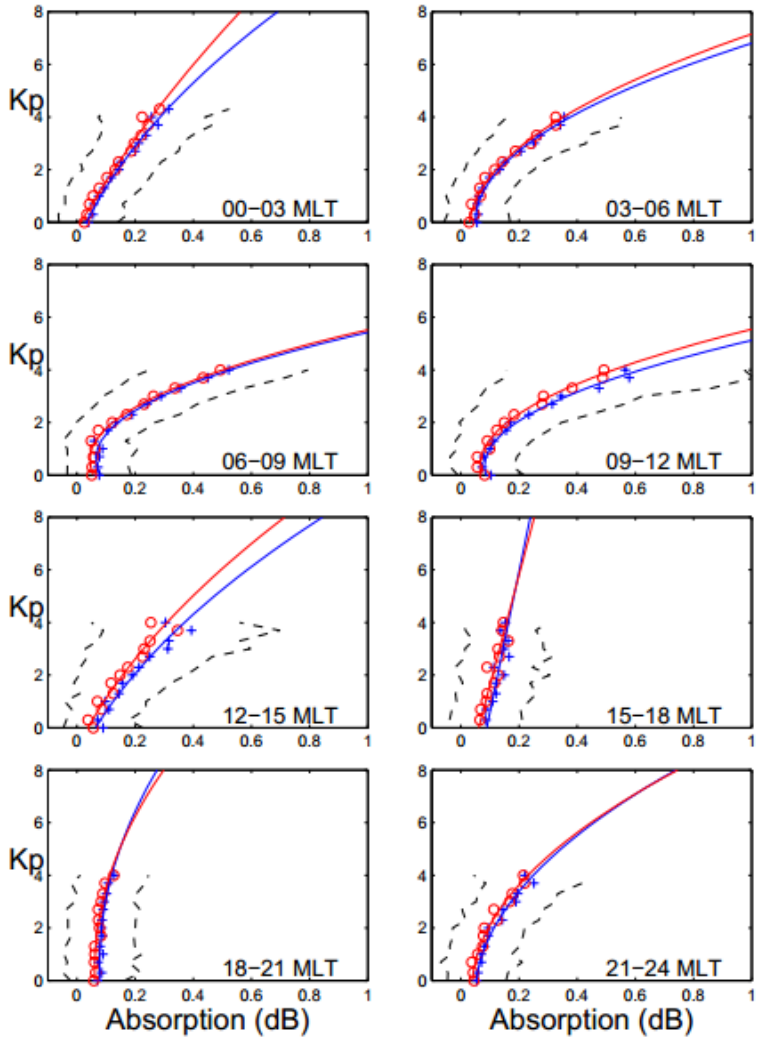

Figure 3.6: Local time plots of the median (red circles) and mean absorption (blue crosses) against the K_p. The curves represent quadratic fits to the data points and the black dashed line represent ± 1 standard deviation about the mean [Kavanagh et al., 2004].

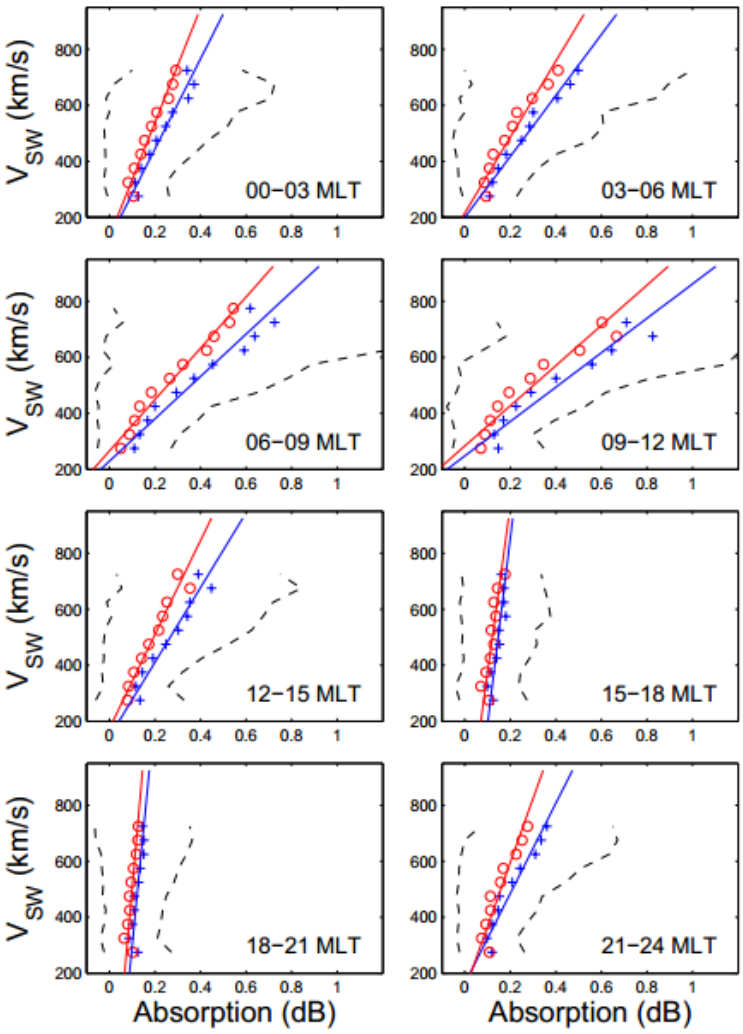

Figure 3.7: Absorption versus solar wind velocity for 8 MLT ranges. Mean and median values are calculated for each 50 km/s bin and straight line fits derived. Dashed lines represent ±1 standard deviation about the mean [Kavanagh et al., 2004].

Chapter 4

Methods

4.1 The SGO riometer network

SGO uses analogical La Jolla riometers. They measure the signal received from the antenna by compensating the signal and measuring the compensation voltage. See the block figure 3.1 of the receiver. The used antenna is a dual half-wave dipole antenna which forms a 60° wide beam towards the zenith of the sky. Frequencies, as well as the coordinates, of the stations can be found in table 4.1. The geomagnetic coordinates presented in the table are computed from the IGRF model for 2008.

Station	gglat	gglon	cgmlat	cgmlon	L-val.	MHz	UT
Hornsund	77.00°N	15.60°E	74.29	108.82	13.1	30.0	21.04
Abisko	68.40°N	18.90°E	65.46	101.47	5.6	29.9	21.31
Ivalo	68.55°N	27.28°E	65.24	108.29	5.5	30.0	21.03
Sodankylä	67.42°N	26.39°E	64.13	106.85	5.1	30.0	21.08
Rovaniemi	66.78°N	25.94°E	63.49	106.11	4.8	32.4	21.11
Oulu	65.08°N	25.90°E	61.75	105.14	4.3	30.0	21.15
Jyväskylä	62.42°N	25.28°E	59.01	103.37	3.7	32.4	21.22

Table 4.1: Geographic and geomagnetic co-ordinates for respective stations, their frequencies and UT at local MLT midnight, IGRF 2008.

4.2 Determining the quiet day curve (QDC)

4.2.1 Automatic method

The original raw data has a resolution of 10 seconds. Antti Kero used one minute median values as the basis in determining the QDC. A sinusoidal curve is fitted to the data from 10 previous days, and forms the quiet-day curve for the 11th day. Note that a day refers to the sidereal day which is a few minutes shorter than 24 hours, approximately 23 h 56 min 4 sec. It tells the Earth's rotation time relative to a fixed distant star, rather than the Sun.

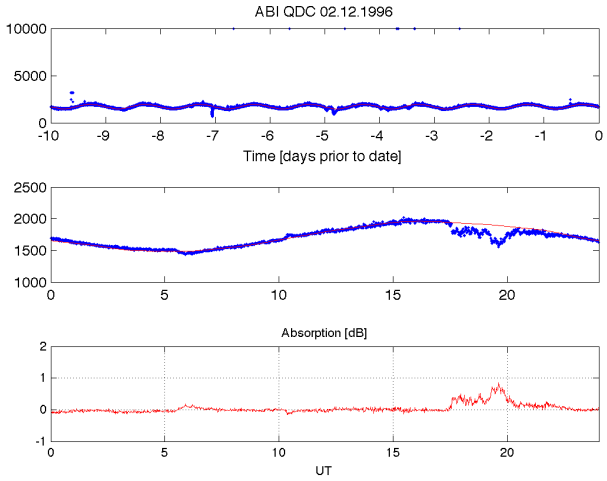

Figure 4.1: An example of the QDC determination using the automatic method. The top panel show the measured power in arbitrary units from 10 previous days. The middle panel shows the raw data as a function of UT from the day the QDC is applied to. The bottom panel shows the corresponding absorption in decibels [dB] as a function of UT. The data is from 1996 from Abisko station.

Figure 4.1 shows an example of the method. The data is from Abisko 02.12.1996. The top panel of the figure shows the raw data in blue line from ten previous days. The red line is the fitted quiet-day curve. The middle panel shows the raw data from the day which the QDC is used on and the lower panel shows the corresponding absorption calculated using equation 3.1.

4.2.2 Manual method

Another method to determine the QDC is to manually fit a pre-determined curve to the raw power data. This is done by manually setting the level of the curve for

each day. When the QDC does not fit to the data any more, it will be re-evaluated. Several people in SGO have been responsible for the manual scaling, so personal preferences may be visible in the absorption.

4.3 Defining an event

In short, the criteria used in finding the absorption events are the following:

1. The minimum magnitude of an absorption event is 0.5 dB.
2. The minimum distance of two events is 15 minutes.
3. The maximum magnitude for an event is 10 dB.

The absorption data has background noise due to interferences. The lower limit for the magnitude of an absorption event has to be set above the average level of background noise. This is not straightforward because sometimes there might be an offset in the level of the calculated absorption because of uncertainty in QDC determination. We chose 0.5 dB for this limit. The decision was based on Tero Raita's (SGO) and Anita Aikio's (Oulu university) suggestion.

The duration of an event usually varies from minutes to a few hours. In extreme cases absorption can be enhanced for several days. We chose the minimum time between two events to be 15 minutes. This enables us to find most of the short-term events. Longer events will be detected multiple times, due to the method used for finding the events. This should be taken into account when interpreting the results.

We chose the upper limit for an event to be 10 dB. Absorption events higher than this can occur but they are rare. Larger values are usually caused by interferences. Figure 4.2 shows an example of the events found using these criteria. The data is from the Abisko station, and the absorption is calculated based on the automatic QDC method.

4.4 Corrections to the data

The automatic absorption data occasionally has big disturbances lasting for several days. Also there can be an offset in the baseline level when the QDC doesn't fit

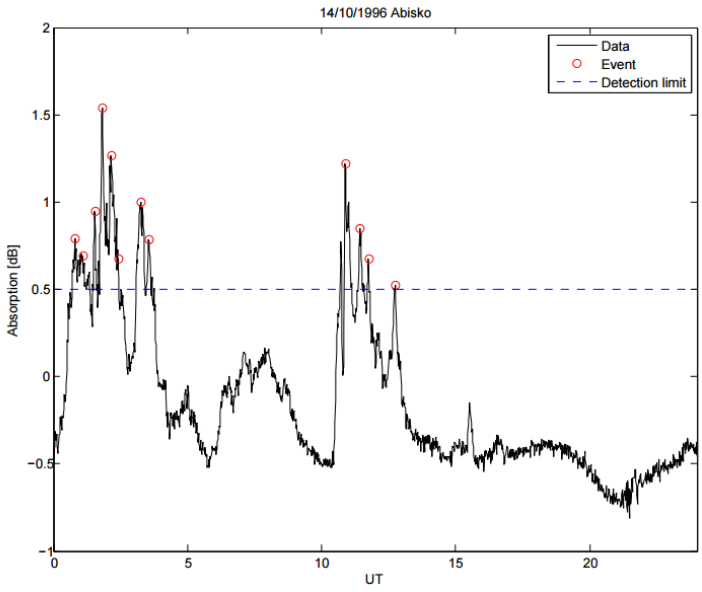

Figure 4.2: An example of the automatic data from the Abisko station. The black line shows the absorption data, the events found with the criteria are marked with red circles and the blue dashed line shows the detection limit. The absorption is calculated based on the automatic QDC method.

well to the data. Because the applied frequencies are also used for military communication, local transmitters can saturate the receiver from time to time. Also the weather can have an effect on the measured signal. For example the heating of the device in summer or high snow cover during winter can cause interference. Another notable problem with the automatic method is that during snowfall the intensity of the signal reduces constantly, and the method can't change as rapidly to compensate it. This shows up as false increased absorption.

We have experimented with certain corrections to the automatic data set. The corrections we tried were:

1. Manually removing the days with clear interferences to avoid finding false events.
2. Subtracting the daily median value from the day's data to remove possible offset.
3. Subtracting the daily median value from the days when the difference between the upper and lower quartile is less than 0.3 dB, i.e. when the deviation of the values is small.

The last two corrections had very little effect on the results, so we decided to manually go through the data and remove the data from days when large interferences were visible.

Due to the problems with the automatic QDC method, we also decided to remove data from the winter months of the years 2000 - 2003. The start and end days of these periods were identified by checking the daily plots of the absorption data, which Antti Kero (SGO) had provided. Many real absorption events are lost because of this, but the anomaly of the solar cycle maximum years distorts the results so much that we decided it would be best to ignore this data. In the future it could be possible to include parts of the data because the interferences seem to mostly occur during daytime. With some modifications to the QDC method the night time data from these periods could also be included. This issue is further discussed in section 5.2.

Chapter 5

Results

5.1 The data sets

The data sets are based on the two different QDC methods, as discussed in Chapter 4. The automatic data set, i.e. absorption evaluated based on the automatic QDC method, was provided by Antti Kero (SGO). The manual data set, where absorption is manually evaluated, was provided by Tero Raita (SGO). The third data set is derived from the automatic data set. In this data set interferences are removed by replacing the affected data points with NaN-values. The data sets used in this thesis:

1. Absorption data using the automatic QDC method, referred to as the uncorrected automatic data.

2. Absorption data using the automatic QDC method from which interferences have been manually removed, referred to as the corrected automatic data.

3. Absorption data using the manual QDC method, referred to as the manual data.

5.2 Anomaly of 2000 - 2003 in the automatic data set

Figure 5.1 shows the number of CNA events as defined in section 4.3. Data from all seven stations of the riometer chain are included in the figure, though there are some gaps in the data from Rovaniemi and Hornsund. The names of the stations are abbreviations and are marked on the vertical axis along with MLT. The horizontal axis

shows the years with a one month resolution. The resolution of the MLT-axis is 1 hr.

There are some distinguishing features clearly visible during the years 2000 - 2003. An increase in the number of events is visible around 10 - 18 MLT at every station. There are also a few individual months where the number of events is much higher than during the surrounding months, for example in Rovaniemi in the beginning of 1997, in Jyväskylä late 1998, and Hornsund from the year 2011 onwards. These isolated incidences are local interferences and are discussed in Chapter 7.

However, the anomaly of 2000 - 2003 is visible at all stations in different latitudes, so the cause cannot be local interference. Figure 5.2 shows a close-up of these years. There one can easily see that the increase in absorption is concentrated on certain months, typically the winter months starting around October and lasting till the end of April. This anomaly is detected during the maximum years of the solar cycle, so the activity of the Sun may play a part in this. Though it seems that the absorption is increased during these years, this is actually not the case. The activity we see here is just radio frequency interferences, falsely interpreted as absorption. Figure 5.3 shows the number of absorption events during the years 1997-2013 in the corrected automatic data. The used scale is the same as in figure 5.1. There are still some interferences present, but the majority of them is removed.

Figure 5.4 shows the number of events during years 1997-2012 in the manual data. Here the winter months of years 2000-2003 do not have the same clear increase in events as the uncorrected automatic data. There are some gaps in the data, especially in Hornsund, where data has been removed because of interferences. This will also be discussed more thoroughly in Chapter 7.

5.3 Yearly distributions

Figure 5.5 shows the normalized number of CNA events per year in the automatic data set. The normalization was done by dividing the number of events each year n by the number of data points that year N. Because the minimum time between two events is 15 min and the data is in 1-min resolution, the total number of data points has to be divided by 15. The normalization can then be expressed as

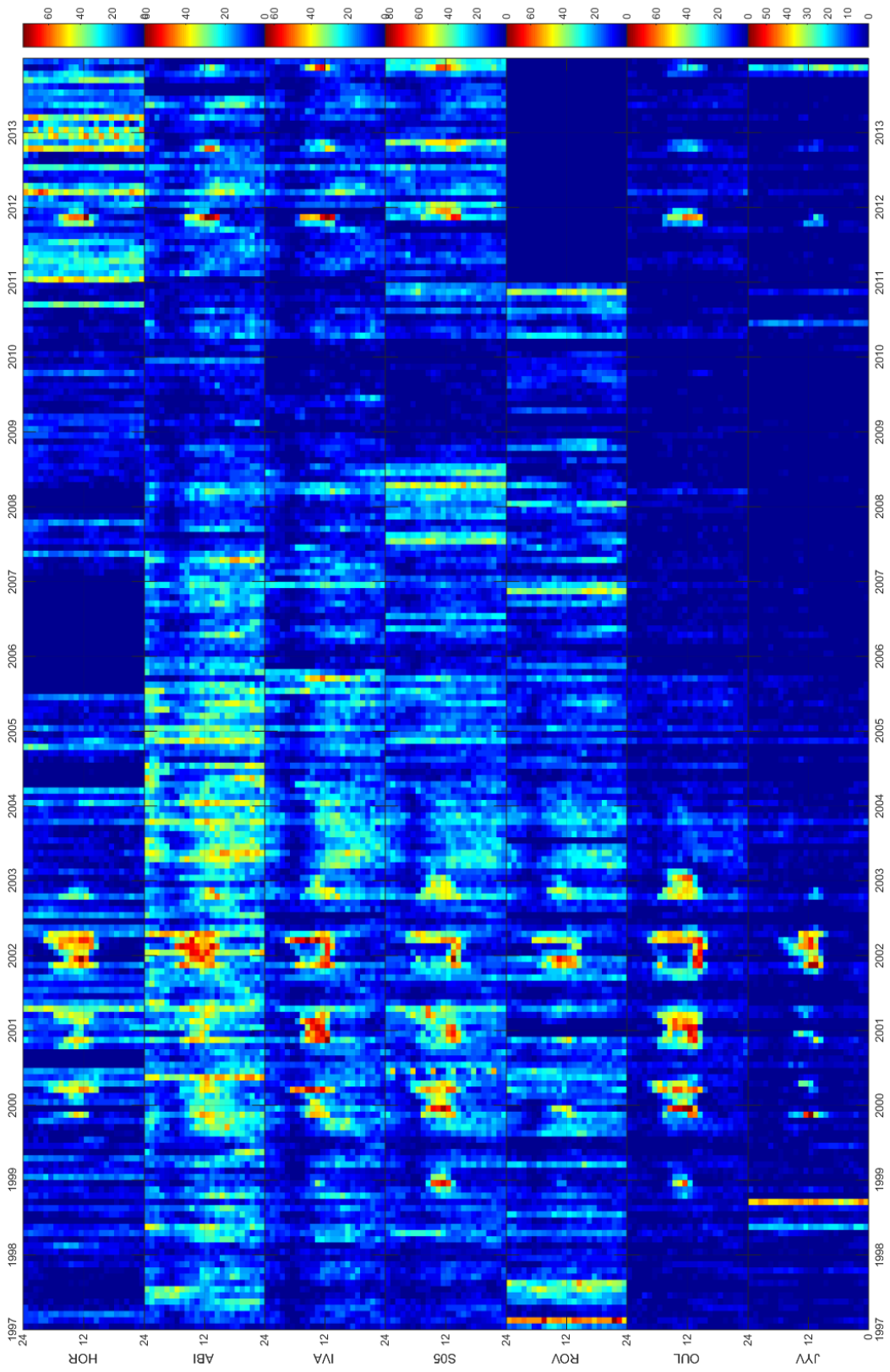

Figure 5.1: Number of absorption events in the uncorrected automatic data set during 1997-2013 as a function of MLT for seven SGO riometer network stations. The resolution of the vertical axis is one month and of the MLT-axis it is 1 hr.

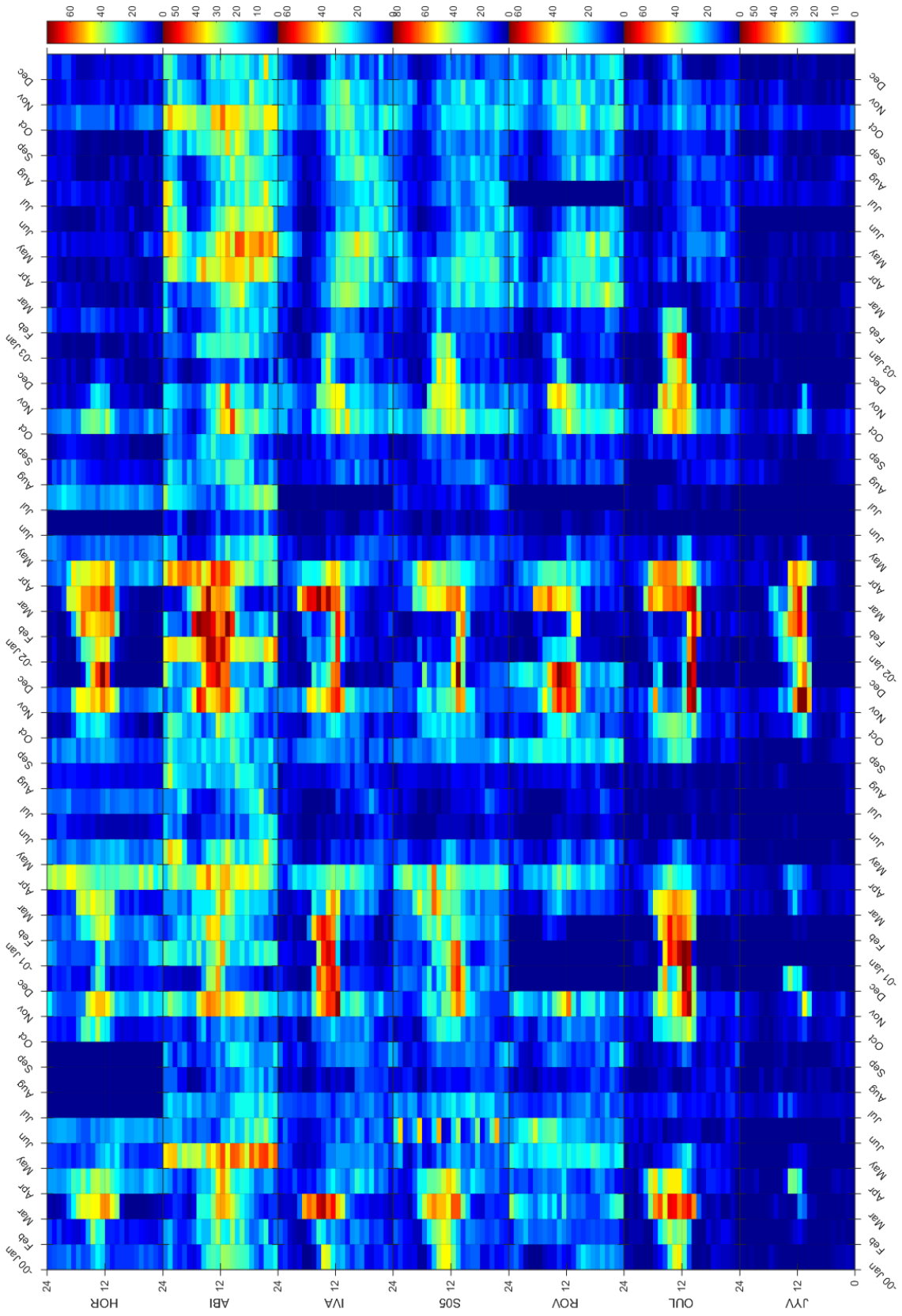

Figure 5.2: Number of absorption events in the uncorrected automatic data set. Close-up on years 2000 - 2003 of figure 5.1.

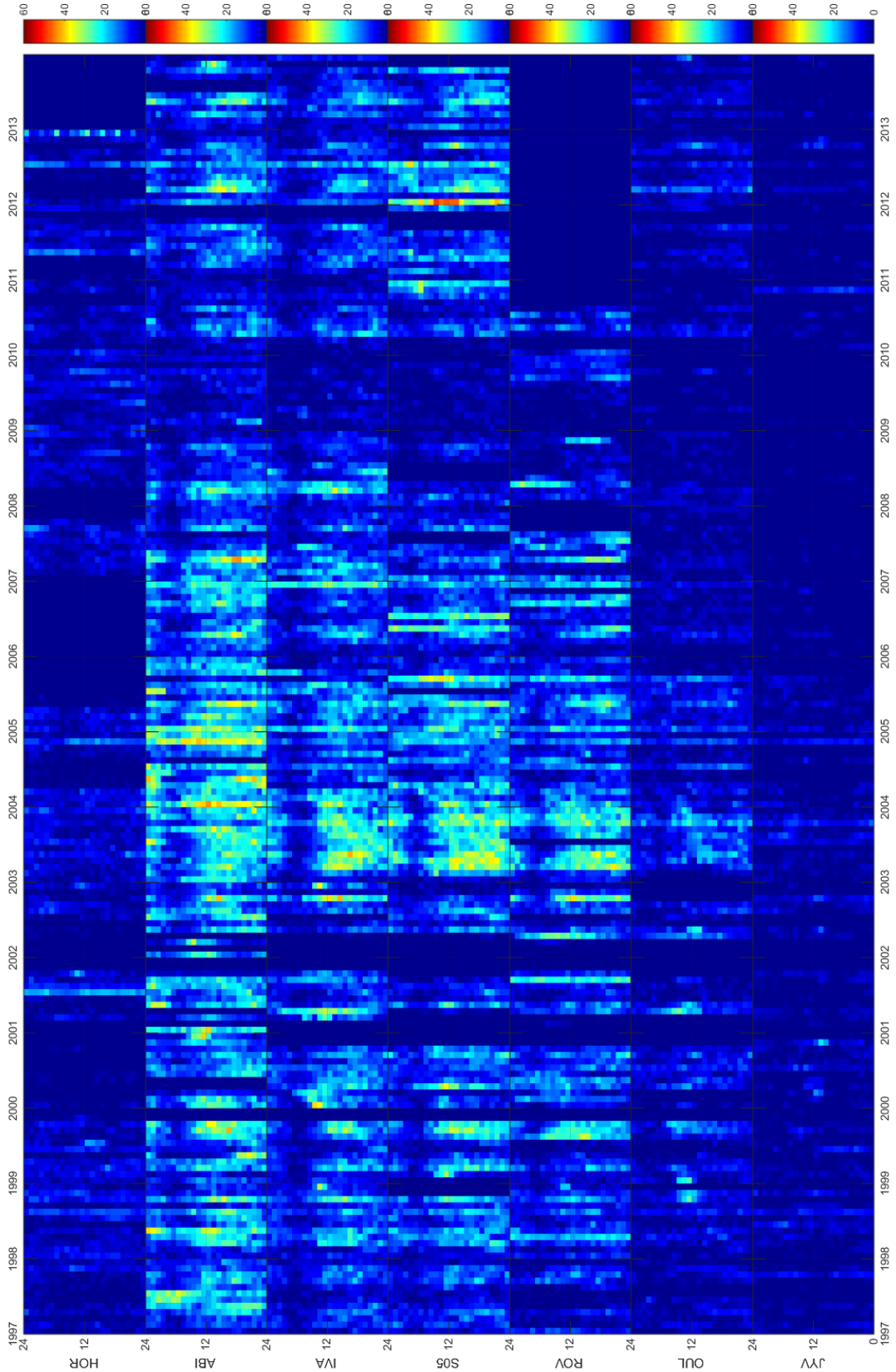

Figure 5.3: Number of absorption events in the corrected automatic data set during 1997-2013 in the same format as figure 5.1.

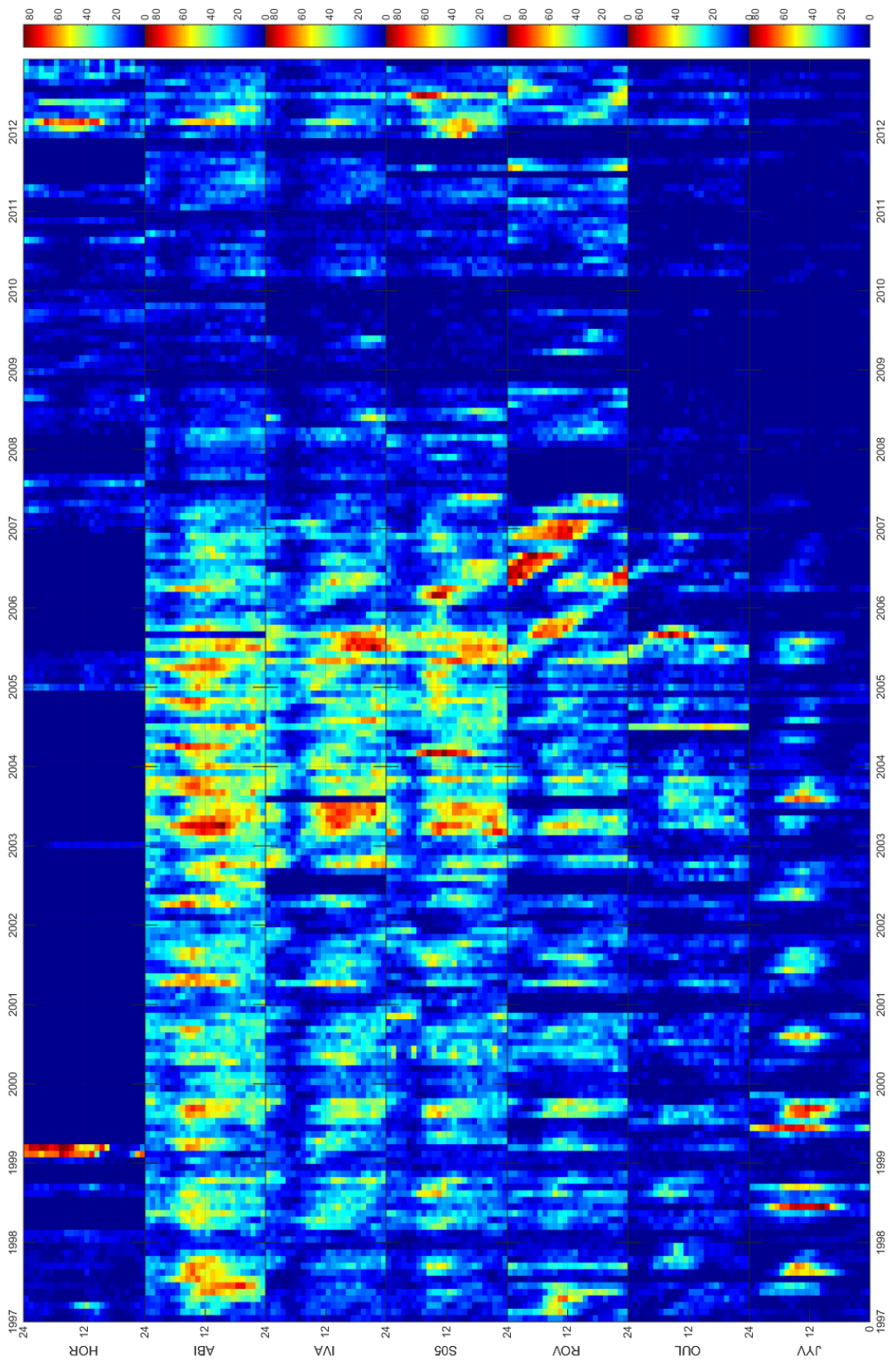

Figure 5.4: Number of absorption events in manual data set, in the same format as figure 5.1.

$$p(year) = \frac{n(\text{year})}{N(\text{year})/15} \cdot 100\ \% \ . \tag{5.1}$$

This gives the percentage of data points, p, exceeding the threshold value (0.5 dB) during one year. The normalization is especially important in figure 5.6, where the days with interferences have been removed and the amount of examined data is significantly decreased.

Figure 5.5 shows the normalized yearly number of events at each station during years 1997-2013 from the uncorrected automatic data. The two top panels show the yearly average sunspot number and K_p index. The plot from the corrected automatic data in the same format is shown in figure 5.6. The amount of absorption events has dropped to about a half from the uncorrected data. The most interferences were removed from Hornsund, Abisko and Rovaniemi, but the biggest changes are seen in Hornsund and Rovaniemi. The distribution of Abisko is not changed by much. The least interferences were removed from Ivalo, Sodankylä and Oulu. Their distributions have not changed much. The change in Jyväskylä's distribution is also quite big. This is because the number of events is very small at the station. Even after the attempted clean-up Hornsund still has many interferences left in the data and its distribution is significantly different from the other stations.

In the corrected automatic data (fig. 5.6) all the stations, excluding Hornsund, have very similar behaviour. Their minimum year is 2009. The years after the minimum have less events than the years before (1997-2008). The K_p index (second panel) has the same decrease. Ivalo, Sodankylä, Rovaniemi and Oulu also have the same maximum year 2003, which is also the maximum of the K_p index. In Jyväskylä there are very few absorption events, which makes the statistics poor. Based on visual analysis, correlation of the number of events with the yearly average sunspot number (top panel) is not as good as with the K_p index. The sunspot maximum year is 2000, after which the activity smoothly decreases until the minimum year 2008. The sunspot maximum is not visible in the amount of absorption events, and the sunspot minimum occurs a year before the absorption minimum.

The yearly distribution of events from the manual data set from years 1997-2012 is shown in figure 5.7. There are five years missing from Horsund, so it's impossible to say much about it. Abisko, Ivalo, S05, Rovaniemi and Oulu have very similar features to the corrected automatic data. All stations, except Hornsund, have a minimum in 2009. The maximum in Abisko, Ivalo and Oulu is in 2003, and in

Sodankylä in 2005. In Rovaniemi there is a local maximum in 2003 but the year 2006 has the most events. Jyväskylä on the other hand has its first maximum in 1998-1999 and a secondary maximum in 2003. Also the manual data set correlates with the K_p index better than with the average sunspot number.

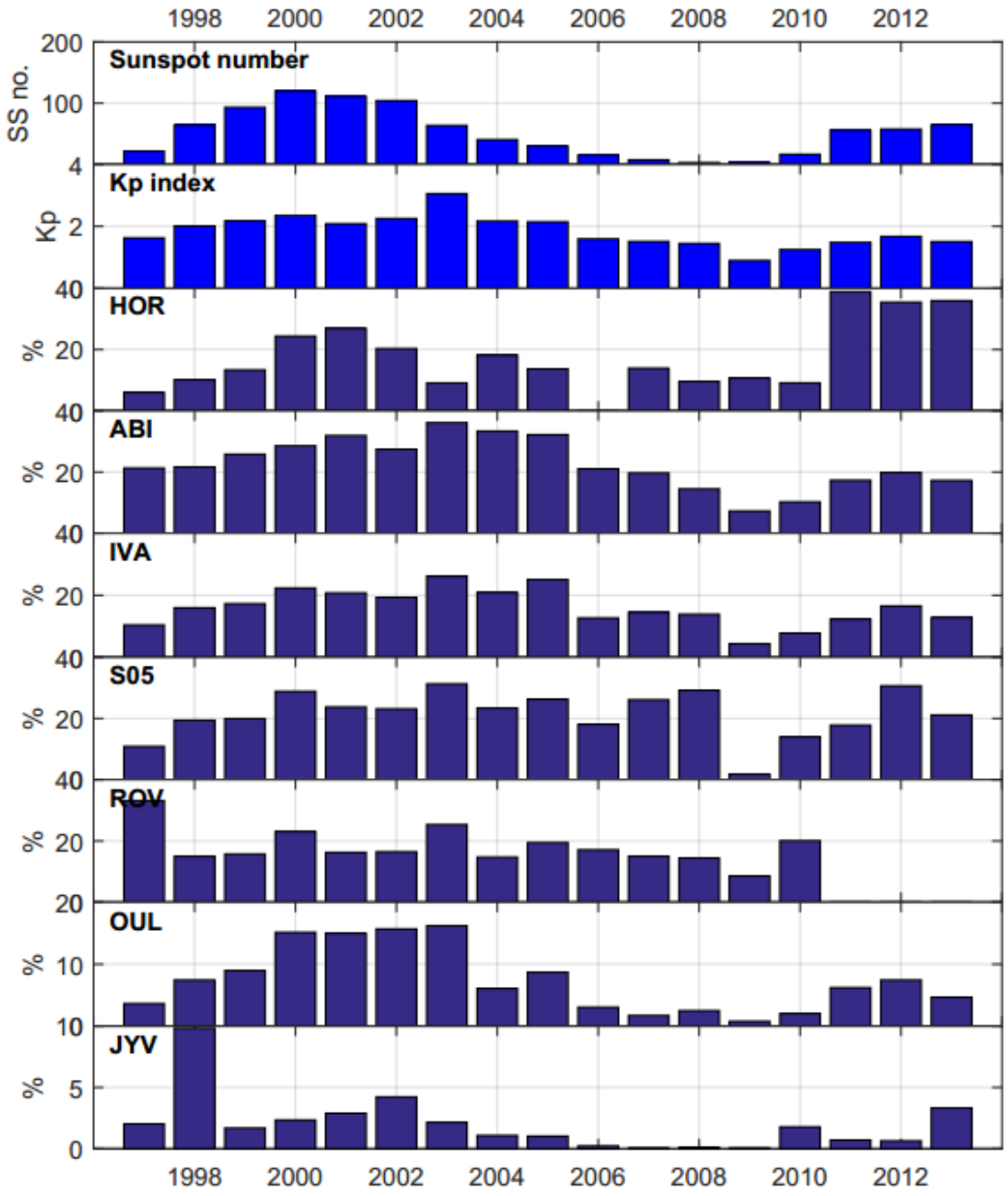

Figure 5.5: Yearly average sunspot number and K_p index and the normalized number of CNA events from seven SGO riometer stations from 1997-2013 from the automatic uncorrected data.

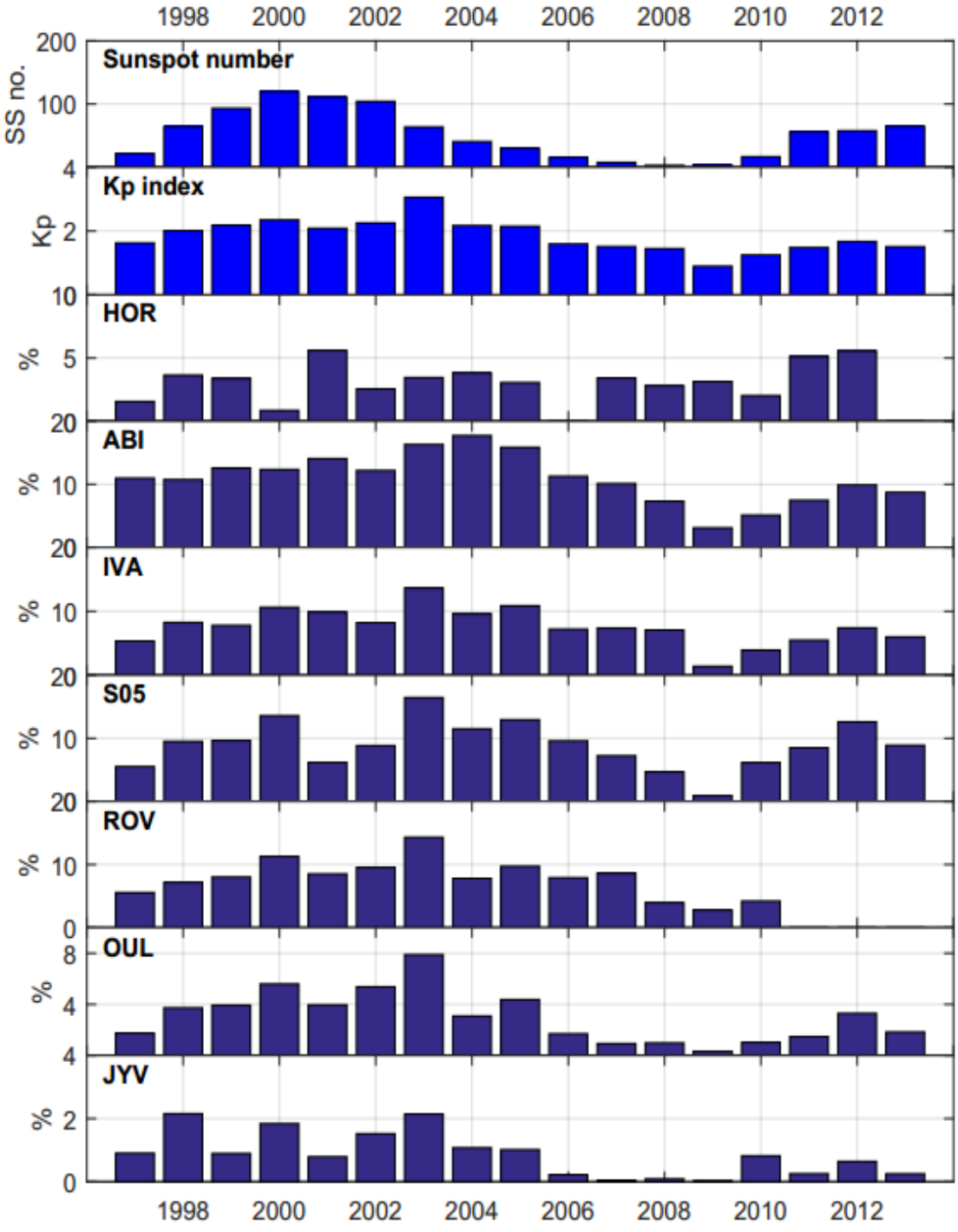

Figure 5.6: Yearly average sunspot number and K_p index and the normalized number of CNA events from seven stations from the corrected automatic data.

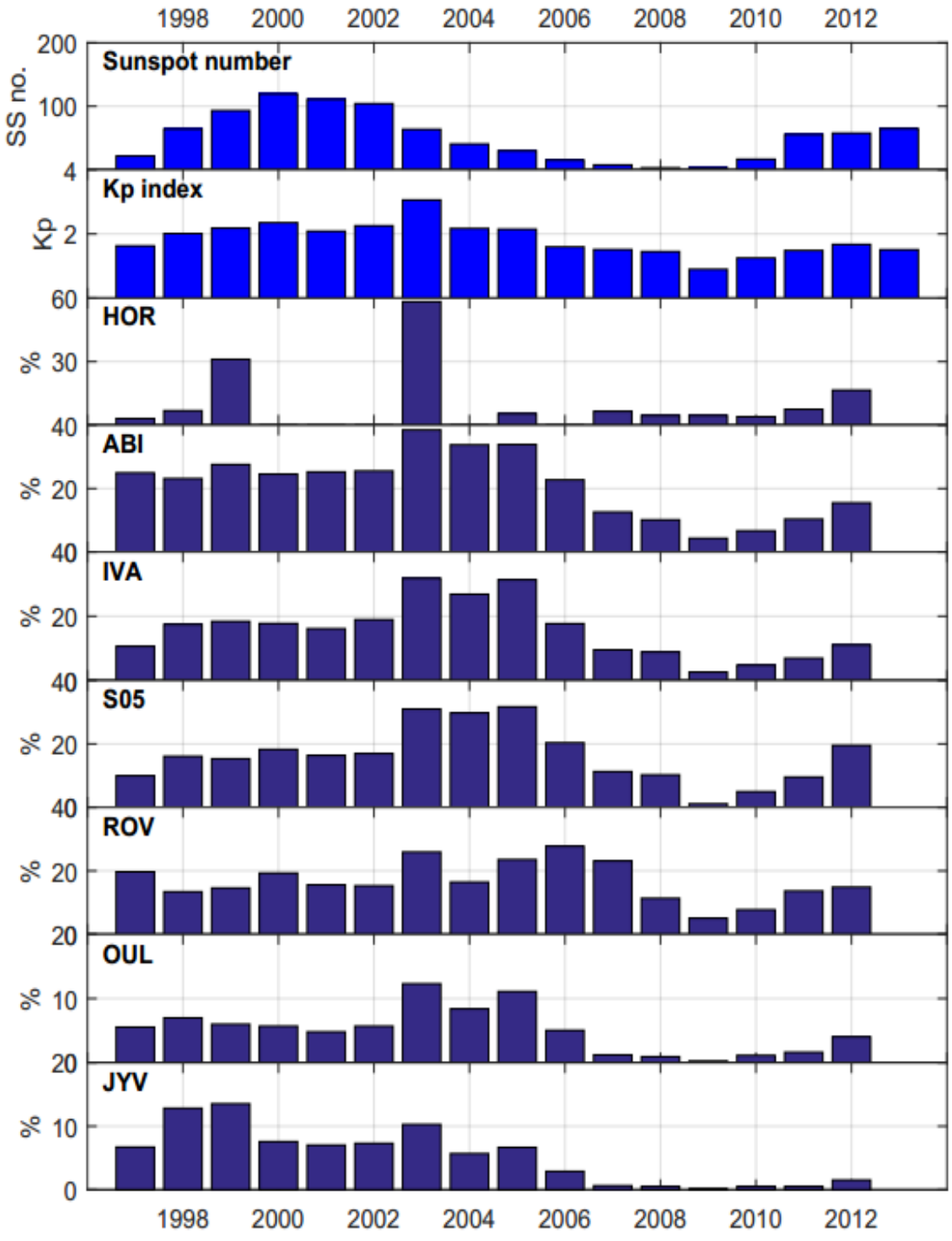

Figure 5.7: Yearly average sunspot number and K_p index and the normalized number of CNA events from seven stations between 1997-2012 from the manual data set.

5.4 MLT distributions

All the MLT distributions from each station from the uncorrected automatic and manual data set are presented in the Appendices. Here I will discuss the MLT distributions from the corrected automatic and manual data, but the figures (5.8 - 5.14) are shown only from the corrected automatic data set, because it is considered the most reliable at this stage. There are a lot of interferences in the measurements from the Hornsund and Rovaniemi stations, so their results will not be discussed deeply.

The normalized number of events, p, is calculated for each year and MLT hour by

$$p(\text{MLT}) = \frac{15 \cdot n(\text{MLT})}{N(\text{all MLTs})/24} \cdot 100\ \% \ , \tag{5.2}$$

in accordance with equation 5.1. This way we get the probability of absorption exceeding 0.5 dB during each MLT hour.

5.4.1 Corrected automatic data

The MLT distribution plots from the uncorrected automatic data are shown in Appendix A. The biggest differences to the corrected automatic data are seen during years 2000-2003. There is a broad peak around 12 MLT, this is very clearly visible in e.g. Oulu. The other years have very similar distributions to the corrected data.

Hornsund

After correction there is very little data left from year 2000 in Hornsund, and year 2013 had to be removed altogether because of almost continuous interferences (see figure 5.8). There is no data from 2006 because the riometer was not operational during that year and the beginning of 2007. Because there probably still are many interferences in the data, the results may not be reliable and will not be discussed here deeply. The distributions do not have many similarities to the other stations. However, during several years between 2004 and 2010 there is a peak close to 09 MLT and another peak close to midnight, similar to, for example, Abisko and Ivalo. The L-value of Hornsund (L=13.1) is a lot poleward from the other stations, e.g. in Abisko L=5.6, so differences are expected.

Abisko

The distributions are shown in figure 5.9. They have surprisingly similar features

almost every year. There is a clear minimum in the early evening sector, though its width varies. The minimum is located around 18 MLT. A clear maximum is not visible every year. In 2000, 2002, 2003 and 2013 the maximum is in the morning sector. During the maximum year, 2003, absorption is detected a bit over 20 % of time at 07 and 08 MLT and during the minimum year the occurrence is less than 6 % at all times.

Ivalo

The distributions are shown in figure 5.10. The L-values (see Table 4.1) of Abisko and Ivalo are almost the same, so similar features are expected to be seen at both stations. The evening minimum is visible every year except in 2001 and 2009. Year 2003 is the maximum year of absorption, when the occurrences are around 20 % during the morning hours, with a peak at 09 MLT.

Sodankylä

The distributions are shown figure 5.11. The early evening minimum is also visible in Sodankylä until 2003, and also less clearly in 2006, 2008 and 2013. The maximum is located around midday. This is most clearly visible from 1997 to 2006. The years 2001 and 2002 have a similar maximum around 11 MLT as in Oulu during the years. During other years the distribution is quite level. The occurrence of absorption is highest in 2003, when absorption is detected around 21 % of time at 03 MLT and 10 MLT

Rovaniemi

The distributions are shown in figure 5.12. The evening minimum around 18 MLT is visible in 1998, 1999, 2002-2005 and 2010. The year 2003 is the maximum year of absorption. Absorption is detected about 19 % of time at 10 MLT. The absorption is at its minimum in 2009, when occurrence is less than 5 % during each MLT hour. There are still interferences in the data from Rovaniemi, so further analysis is not useful. The data from 2011 - 2013 is not available.

Oulu

The distributions are shown in figure 5.13. The early evening minimum is even less clear in Oulu. Generally there are fewer events, about a half of the amount of the stations located in higher latitudes. Absorption is detected less than 10 % of time every year. In 1997 there is a decline in the amount of occurrences starting from 01 MLT. The minimum is at 18 MLT. In 1998 there is a clear maximum at 12 MLT. In 1999 the maximum is two hours later at 14 MLT. The years 2000 - 2002 also have

a midday maximum. Years 2003 and 2004 seem to have two maxima, one before 06 MLT and the other 7 - 14 MLT. In 2005 the maximum is in the early morning at 05 MLT. In 2006 the maximum is at magnetic midnight but several smaller maximums are visible in the morning/day sector. 2011 has a similar declining shape as 1997, and the minimum is at 18 - 19 MLT. In 2012 the maximum is at 11 MLT and minimum at 18 MLT. In 2013 the maximum is, again, at 12 MLT and minimum 17 MLT.

Jyväskylä

The distributions are shown in figure 5.14. Generally there are very few absorption events detected in Jyväskylä, yearly only about a quarter compared to e.g. Abisko. Absorption is detected less than 6 % of time every year. The years 2000 and 2002 have a prominent daytime maximum at 10 MLT also the year 2012 has a similar distribution. This implies that there is about 11-year cycle visible in the MLT distributions. Because of the small amount of events during some years, e.g. 2007-2009, this kind of analysis is not always possible.

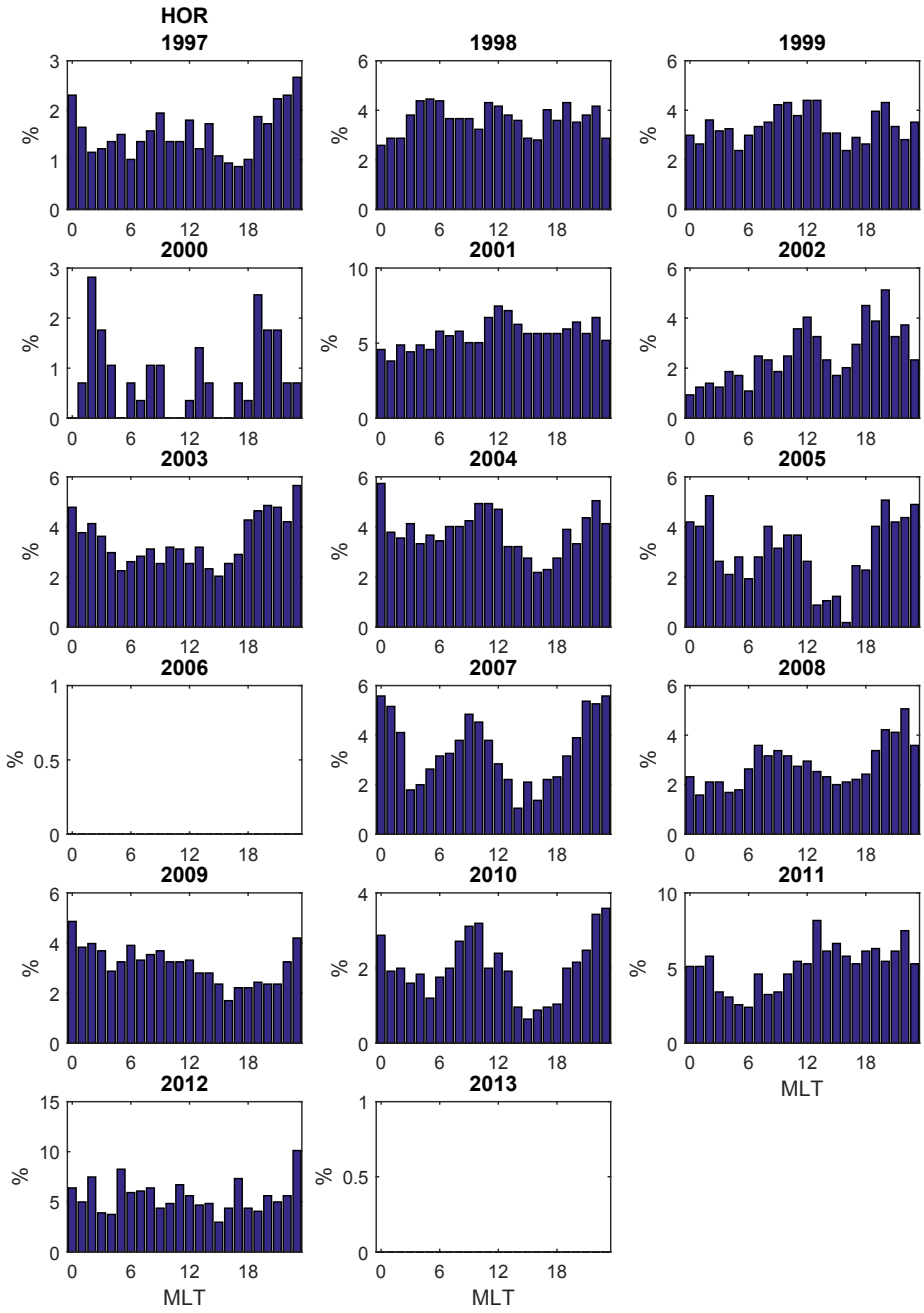

Figure 5.8: Corrected automatic data, Hornsund. Normalized MLT distributions of the number of CNA events. The resolution of the time axis is 1 hr. Note that the scale of the vertical axis is not fixed and can change a lot between different years.

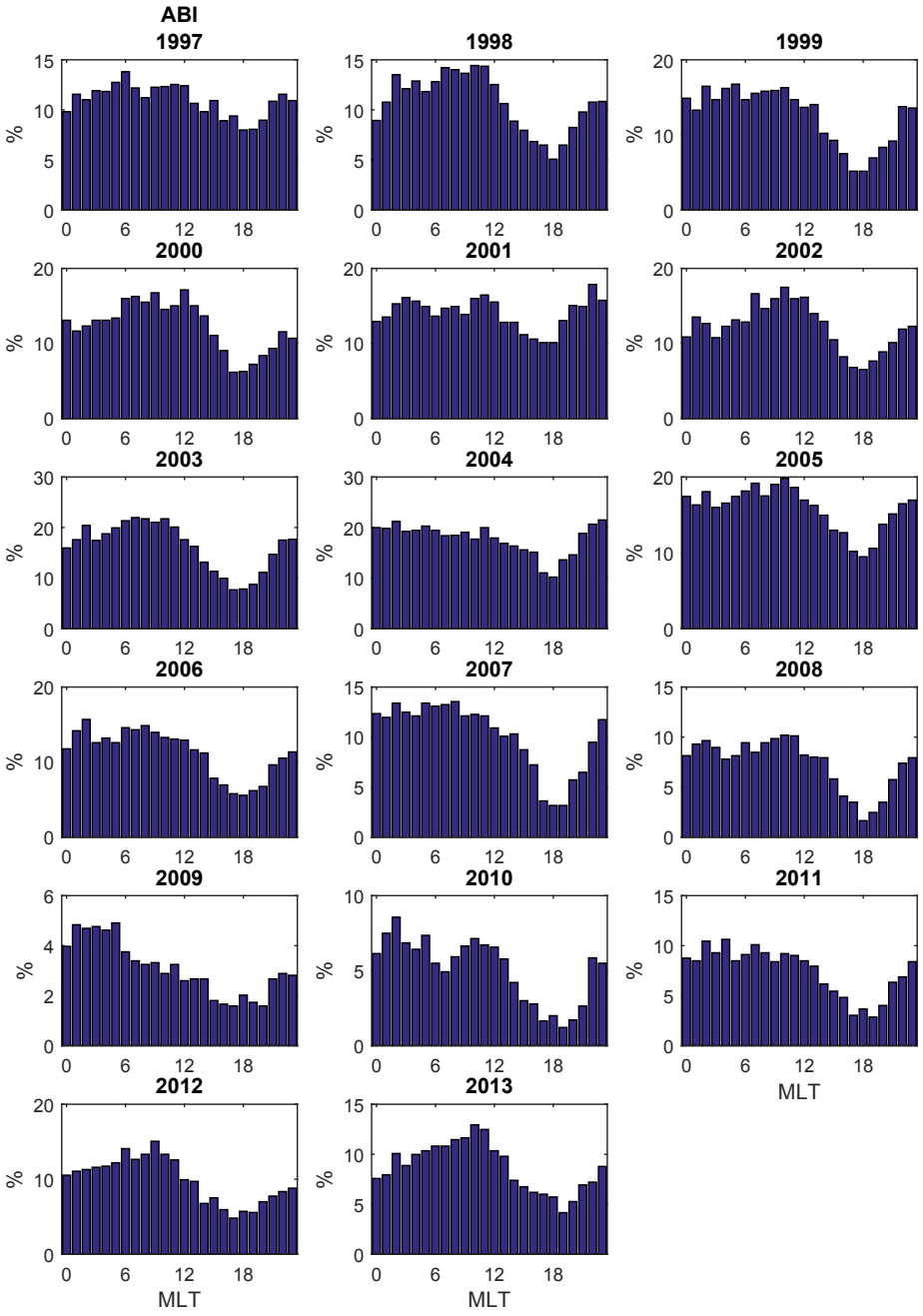

Figure 5.9: Corrected automatic data, Abisko. Normalized MLT distributions of the number of CNA events. Note that the scale of the vertical axis is not fixed and can change a lot between different years.

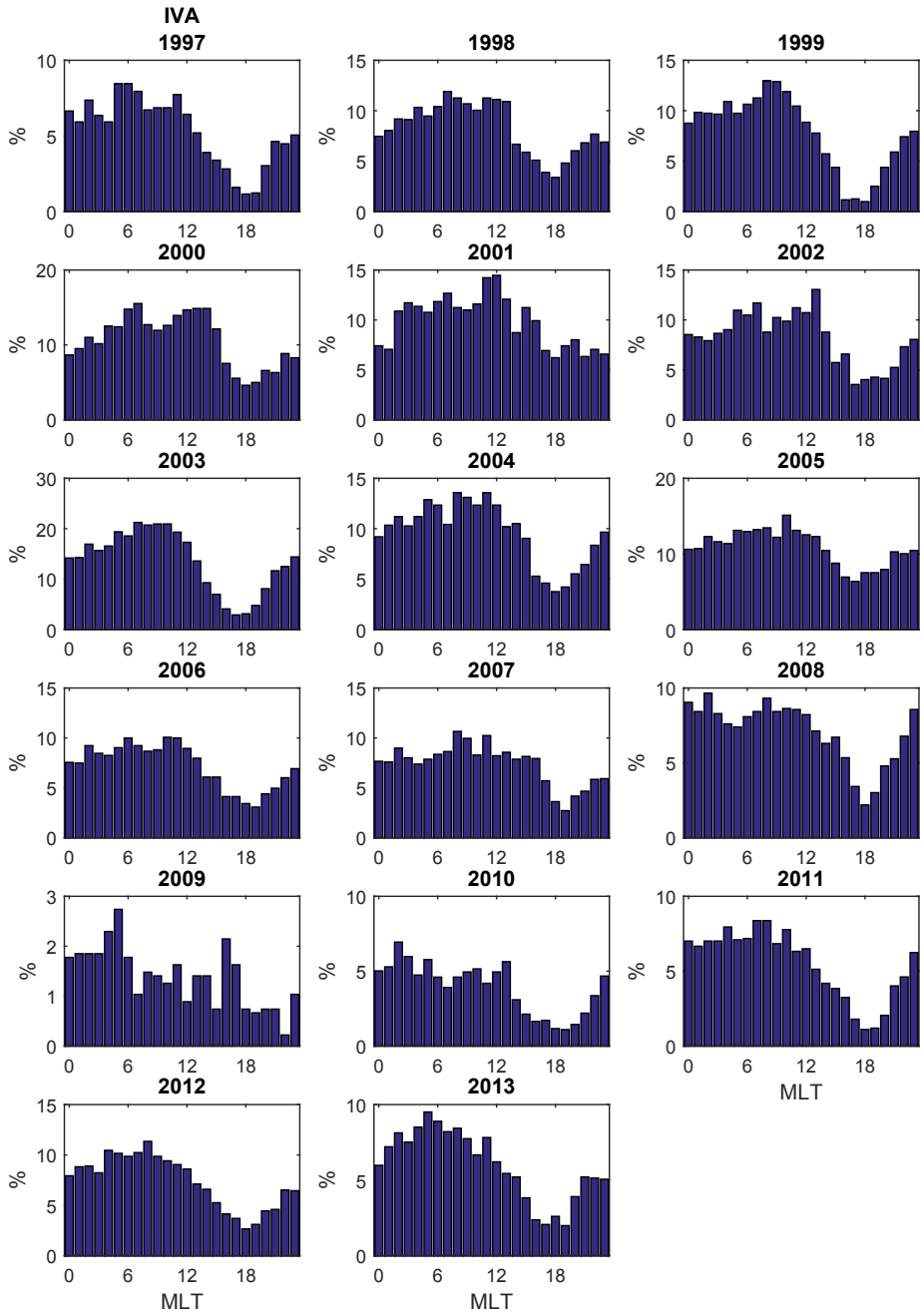

Figure 5.10: Corrected automatic data, Ivalo. Normalized MLT distributions of the number of CNA events. Note that the scale of the vertical axis is not fixed and can change a lot between different years.

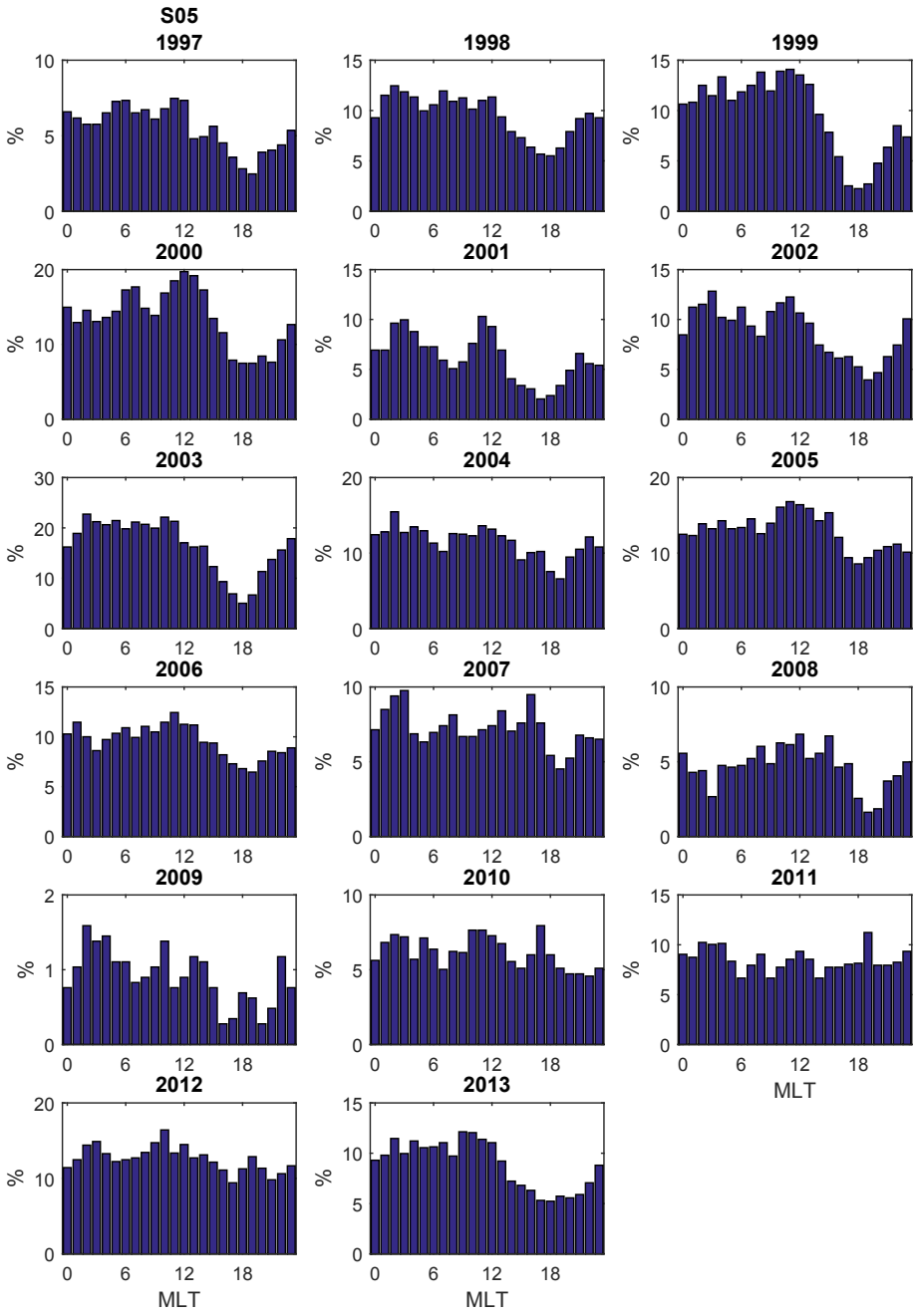

Figure 5.11: Corrected automatic data, S05. Normalized MLT distributions of the number of CNA events. Note that the scale of the vertical axis is not fixed and can change a lot between different years.

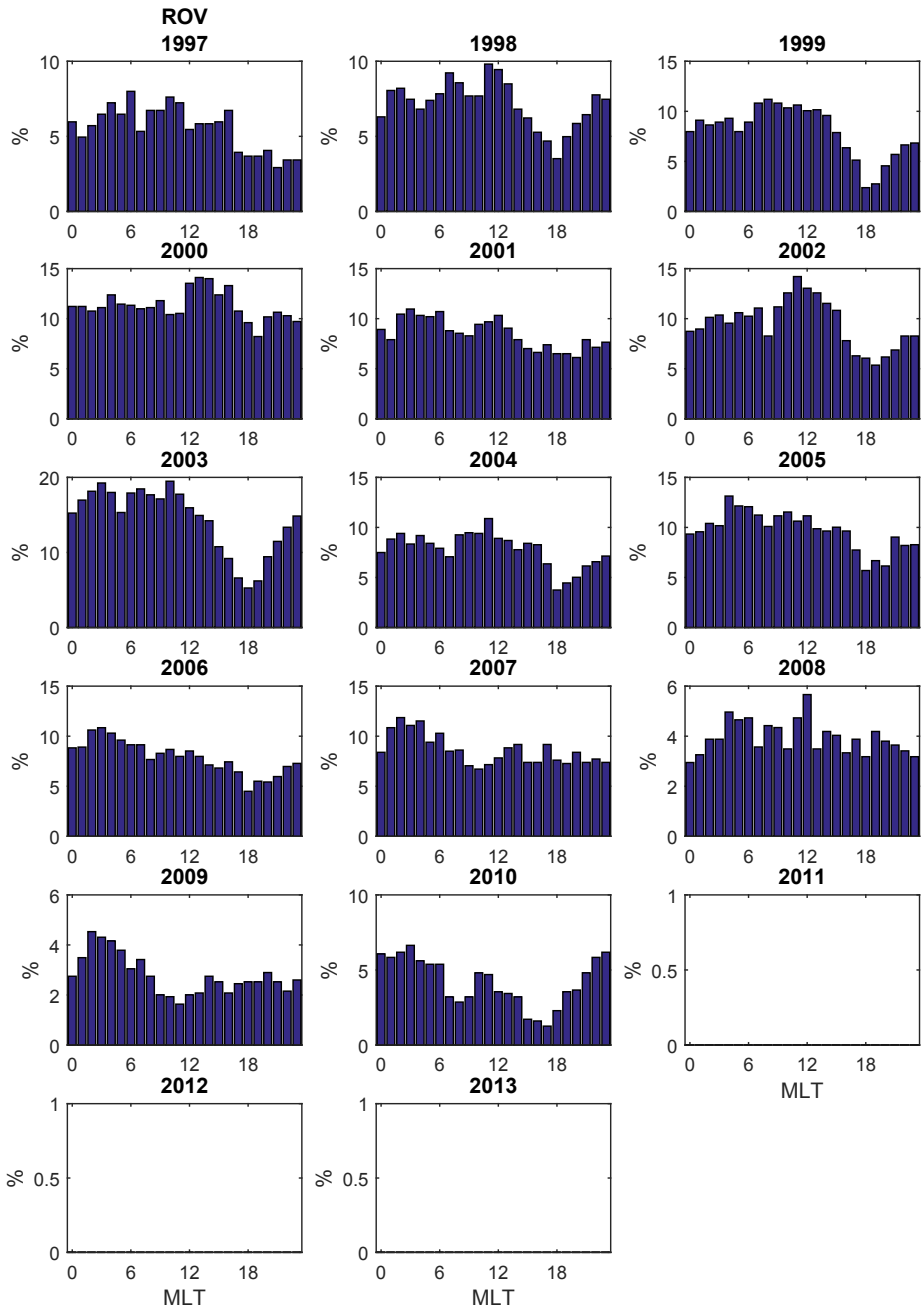

Figure 5.12: Corrected automatic data, Rovaniemi. Normalized MLT distributions of the number of CNA events. Note that the scale of the vertical axis is not fixed and can change a lot between different years.

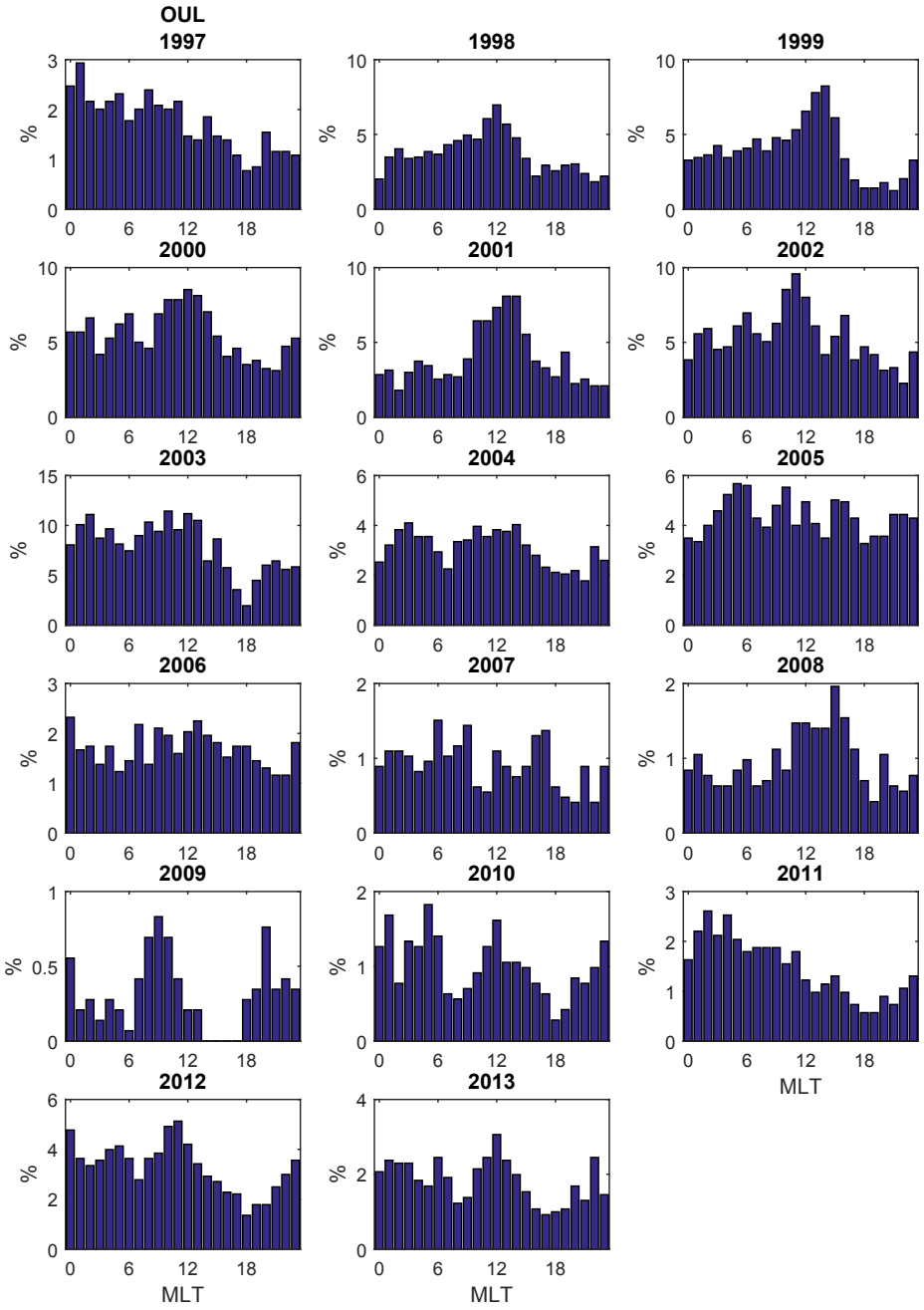

Figure 5.13: Corrected automatic data, Oulu. Normalized MLT distributions of the number of CNA events. Note that the scale of the vertical axis is not fixed and can change a lot between different years.

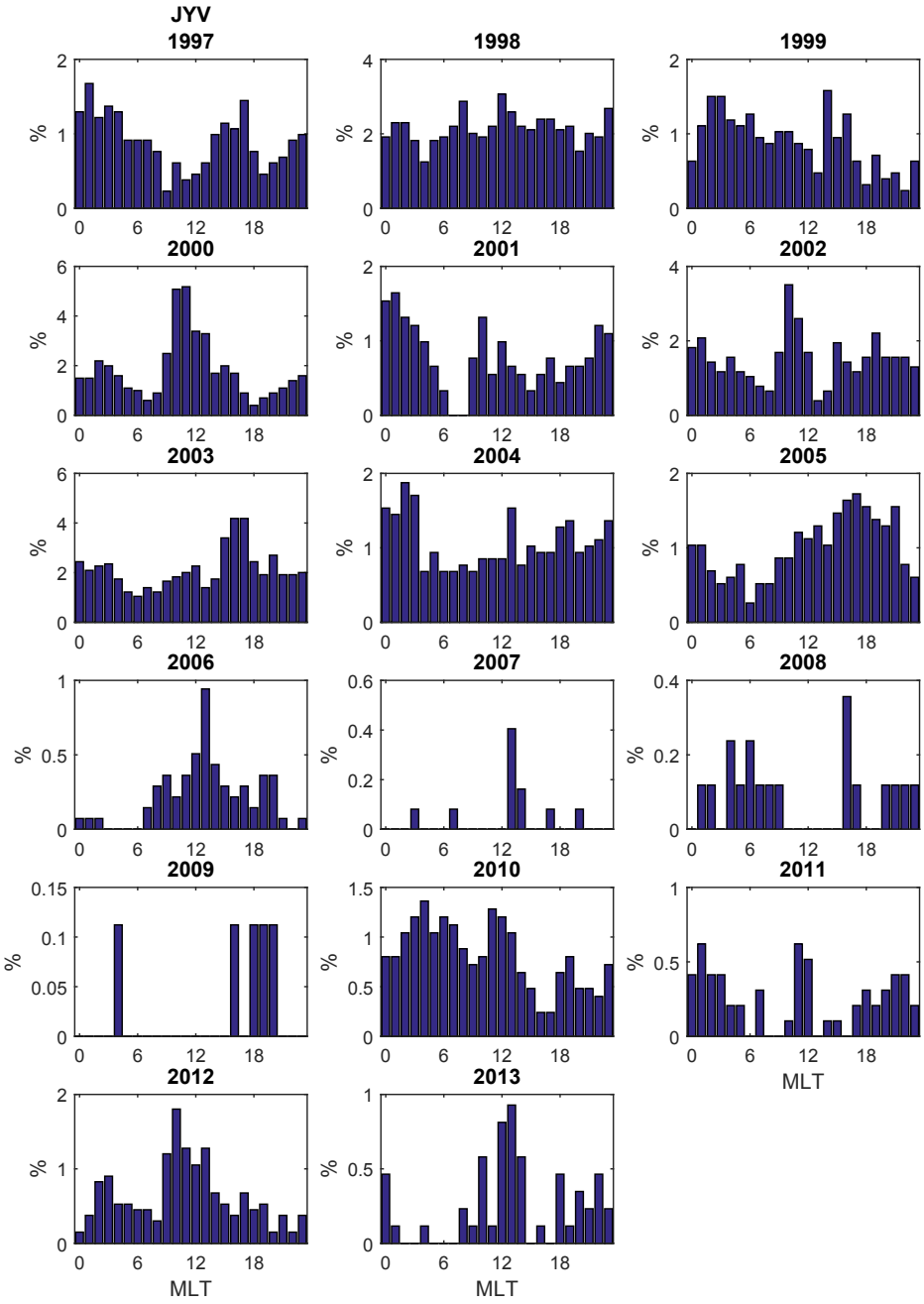

Figure 5.14: Corrected automatic data, Jyväskylä. Normalized MLT distributions of the number of CNA events. Note that the scale of the vertical axis is not fixed and can change a lot between different years.

5.4.2 Manual data

All the MLT distributions of the manual data set can be found in Appendix B.

Hornsund

In 1997 and 1998 there is a prominent noon maximum that is not visible in the automatic data set. In 1999 there is a minimum at 04 - 06 MLT that also was not visible in the automatic data. However, the years 2005 - 2009 have quite similar distributions compared to the automatic data. In 1999 and in 2003 the percentage of occurrences is three times higher than rest of the years.

Abisko, Ivalo

The years 1997-1999 have quite a uniform structure. The occurrences slowly increase until 13 - 14 MLT, after which they drop suddenly. 2000-2001 have at least two maximums, the first at 07 MLT and the second at 14 MLT. In 2002 the occurrence rate is highest in the morning sector 07 - 09 MLT. 2003 has a broad maximum expanding from 07 MLT to 16 MLT. From 2004 forward the distributions have a similar shape as in the automatic data. Most years in the Ivalo station are similar to the corrected automatic data. Only the year 2009 is significantly different.

Sodankylä

Differences to the automatic data are quite clear. The day time maximums in 1997 and 1998 are rather prominent, whereas in the automatic data they are not visible. 1999 and 2003 resemble the corresponding years from automatic data very well. The percentages of occurrences are also almost two times higher until 2009.

Rovaniemi

It is difficult to find any similarities with the automatic data set. The occurrence rates are at lest two times higher. The quality of the data from Rovaniemi is unreliable and most of the occurrences may be caused by interferences.

Oulu

1997 and 1998 show most occurrences in the afternoon sector, just after 12 MLT, whereas years 1999-2002 show a preference to the morning sector. From 2003 until 2006 the maximum is shifted towards afternoon. This kind of behavior is not seen in the automatic data. From 2007 onwards the distributions look more similar to the corrected automatic data and the occurrence percentages are almost the same. It should be noted that Tero Raita has verified the manual data set from 2007 on-

wards, so these years should have a better correlation.

Jyväskylä

There is a strong preference to day time occurrences until 2007 when the maximum starts to shift to the afternoon/evening sector. This overpowering feature is not visible in neither of the automatic data sets. The percentages are also a lot higher in the manual data, in some cases over ten times, 1999 for example.

Chapter 6

Discussion

6.1 Quality of the data

The quality of the data received via riometer measurements is variable. The antenna is sensitive to changes in orientation and snow coverage, and the receiver is sensitive to temperature changes and interferences by terrestrial RFIs (Radio Frequency Interference) and thunderstorms.

Another crucial issue is the determination of the QDC. In SGO two methods are used. One is the manual method where the level of the predetermined QDC is chosen manually. The strength of this method is that when the QDC clearly doesn't fit to the measurements, it gets re-evaluated. Its weakness is that the results may vary according to who is doing the scaling. At SGO the quality of the manually scaled absorption data was not rigorously verified between 1997 and 2007.

The other method is the automatic method which was discussed in Chapter 4. It determines the QDC similarly for all the data, but the fit of the QDC to data is not evaluated during the process. This leads to problems like the anomaly in 2000-2003.

6.2 Effect of interferences

The riometer device is very sensitive to changes in temperature and the orientation of the antenna. The temperature of the device in different stations has been measured from 2005 onwards, but before that year no such measurements are available. High snow coverage changes the contact between the antenna and the ground, resulting in changes in the received signal. Besides military communications, other

devices using the same frequencies and, for example, thunderstorms can also cause interferences. Physical damage to the antennas by wildlife is also possible. These kind of factors can explain the isolated cases of increased absorption in the figure 5.1.

The apparent anomaly in CNA during 2000 - 2003 is caused by the automatic QDC determination method. The method is explained in Chapter 5.1. It uses the raw power data from ten previous days to determine the QDC. When a long-term radio interference is measured for several consecutive days, it begins to alter the shape of the QDC. Normally the QDC is a smooth curve, but during the anomaly its shape changes dramatically. After a few days with the radio interference, the method begins to compensate for the increase in measured power. This can be seen as a bulge appearing in the day section of the QDC.

Figure 6.1 shows an example of this behaviour. The difference is clear if compared to the "well-behaving" QDC example in figure 4.1, where the plot of the measured power in the top panel is a smooth, periodic curve. In the top panel of figure 6.1 there is a reoccurring sharp jump in the value of the measured power caused by a burst of radio interference which saturates the receiver. This interference has been detected for over ten consecutive days in the example. The middle panel shows the measured power (blue dots) and the QDC (red line) for the day. Usually the QDC is a smooth curve, but in this case there is a large bulge between 06 - 16 UT. The corresponding absorption is shown in the bottom panel. The absorption is highest when the interference begins, at 06 - 09 UT, and when it ends at 13 - 16 UT. This happens because the QDC is too high and after the RFI ends it still remains too high for a few hours.

Figure 6.2 shows the absorption plot from the same day and station (9th of January, Oulu) from the manual data set. There is no absorption (0 dB) detected during the RFI, whereas in the automatic data set figure (6.1, bottom panel) we see absorption values of over 2 dB. This is because in the manual method the QDC curve is not calculated based on the previous days and thus is not affected by long lasting RFIs. Also, the manual data set does not have negative absorption values, unlike the automatic data. If the negative values were included, the period of the RFI would be seen as strong negative absorption. Some interfered periods have been manually removed from the manual data set by the SGO people responsible for it. This is the case with, for example, the data from Hornsund. Data from multiple years is missing, whereas in the automatic data set these years are still included.

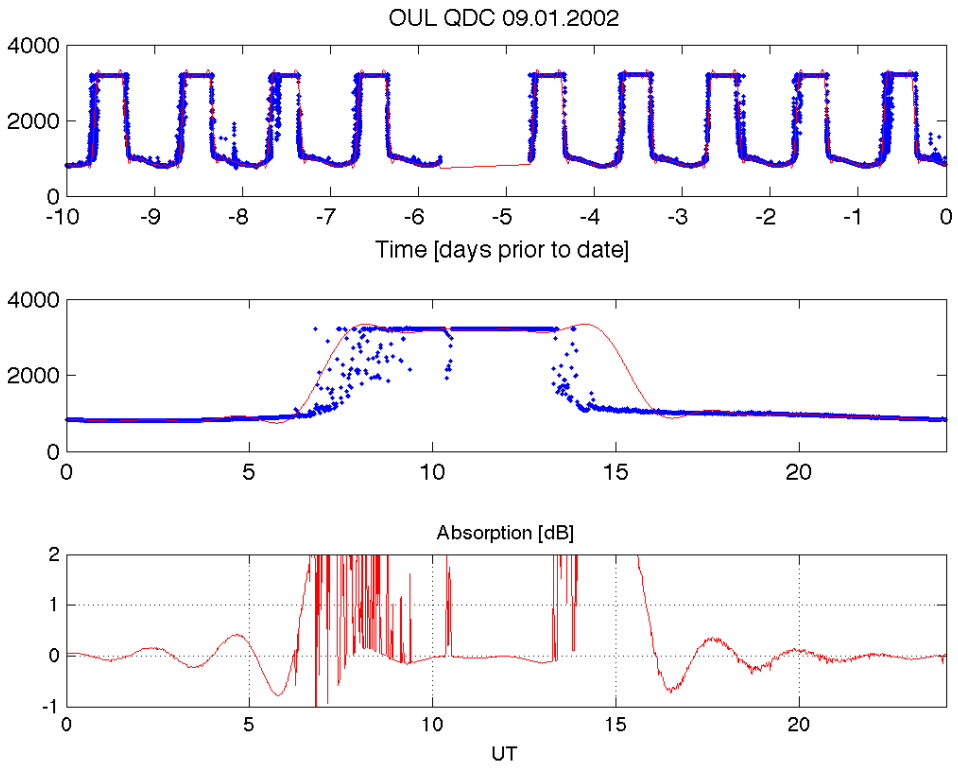

Figure 6.1: Example of badly behaving automatic QDC. The top panel shows the measured power in arbitrary units from 10 previous days. The middle panel shows the measured power (blue dots) from the day the QDC (red line) is applied to. The bottom panel shows the corresponding absorption in decibels as a function of UT. The data is from Oulu, 09.01.2002.

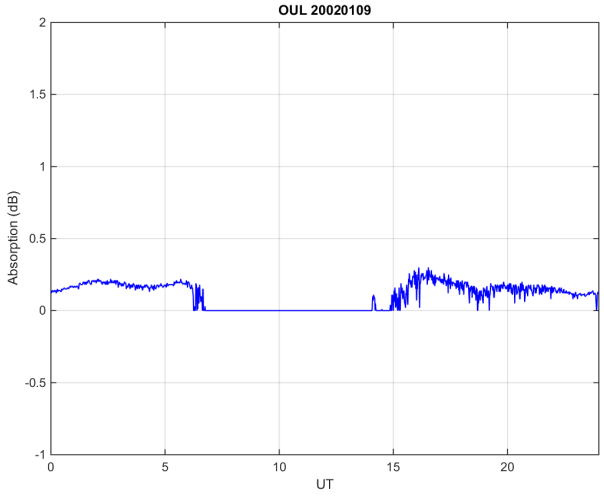

Figure 6.2: The absorption data from Oulu, 09.01.2002, in the manual data set.

Though the anomaly definitely is a curiosity, it is not absorption, and thus not something we want to include in the final results. In my theses we simply ignored the data from the interfered days in the automatic data set. Many real absorption events are lost because of this, which affects the statistical weight. The saturation phenomenon occurs during winter months from October to the end of April. In the corrected automatic data between 2000 - 2003, the results are only based on measurements from May to the beginning of October. The saturation effect occurs typically on the day side, so some night side data could be retrieved if the automatic QDC determination is developed further to ignore the data points from when the detector is saturated.

6.3 Yearly distributions and MLT distributions

Because much of my work time was spent on validating the data and experimenting with suitable methods for finding the real absorption events, the emphasis of this thesis is in data validation and analysis. In this chapter I summarize our main geophysical findings and compare them with some earlier research.

We first tried comparing the yearly distributions to the yearly average sunspot number, but later decided to also include the K_p index. The yearly distributions show a periodicity similar to the solar cycle but the correlation is not obvious. There seems to be a few year delay in the maximum absorption year to the sunspot maximum, but there is variation in the maximum year between different stations and different data sets. The absorption minimum is during the sunspot minimum years in every station and in all the data sets. Based on visual analysis correlation with the K_p index is more clear. Its yearly distribution is not so smooth as the yearly average sunspot number and it is a better fit to the distribution of the absorption events. The maximum and minimum years of the K_p index are quite well visible in both the corrected automatic data and the manual data, which gives reliability to our results. In many cases similarity with the K_p index is also visible in the uncorrected automatic data, even though interferences dominate the distributions during some years. Especially Abisko, Ivalo and Sodankylä have very similar distributions to the corrected automatic data. In the future correlation coefficients should be calculated for each data set and the K_p index and sunspot number, so that the correlation can be expressed quantitatively.

The K_p index, as explained in section 2.3.4, describes the level of magnetic dis-

turbances in the Earth's magnetic field. Absorption is a D-region phenomena and magnetic disturbances are due to currents in the E-region, so some similarity between absorption and the K_p index would be expected [Hargreaves, 1969]. Kavanagh et al. [2004] studied the dependence of absorption on geomagnetic parameters, and found correlation between the K_p index and absorption. The correlation is strongest from early morning to midday and weakest in the evening (18-21 MLT), see Chapter 3.3.1.

The relationship between ionospheric absorption and the sunspot number has been studied by e.g. Basler [1963] during years 1957 - 1963. This period included the maximum year and a part of the declining phase of the solar cycle. During that period there was no obvious correlation between the monthly average auroral absorption and the monthly average sunspot number. Also Collins et al. [1961] have studied the average auroral absorption during a whole sunspot cycle using ionosond data and found out that it did not follow the sunspot number exactly, and that the relationship with the planetary magnetic index A_p (or K_p) is stronger.

The MLT distributions are a bit different each year. However, a maximum during the morning hours is visible during most of the years. An evening minimum, which is located around 18-21 MLT, is also visible most of the time. These features can be seen during most years in the automatic data sets and the manual data.

The manual data consistently has more events. This, again, is most likely due to the fact that different people have been responsible for the data. If someone tends to set the QDC too low, a certain offset will appear in the absorption data and false events will be detected throughout the day. If the QDC is consistently set wrong for several days, there will be a kind of "background noise" in the detected absorption events. This would add a constant background to the MLT distributions, because the real events are mixed with a great amount of false events. There is some indication of this in the data. Especially if one compares the years 1997 to 2005 in the corrected automatic and manual data sets. The figures of manual data still show a certain preference to some magnetic times, and similar features can be seen as in the automatic data set. The evening minimum, for example, is visible most years in all of the stations, apart from Hornsund and Jyväskylä. This gives at least some credibility for the data sets and we can assume that most of the events detected are real, even though false ones are definitely present. Tero Raita (SGO) has verified the quality of the manual absorption data from 2007 onwards, so the data from these years should be more reliable than the data from 1997 to 2006. In some stations, Oulu for example, this is visible. The resemblance between the corrected automatic

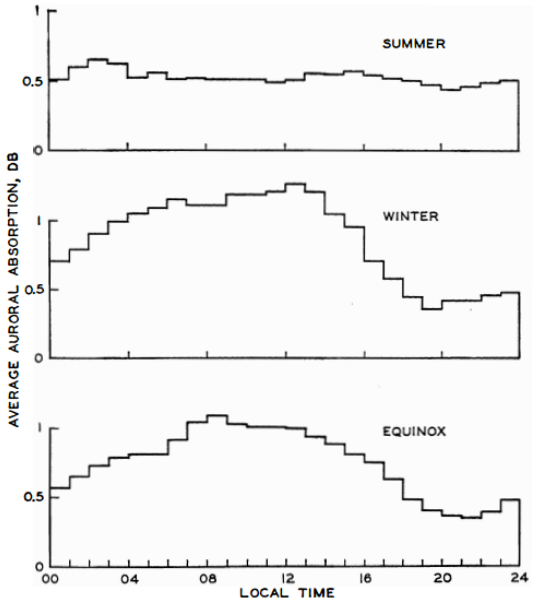

Figure 6.3: The daily variation of auroral absorption at College observed during the 5-year period from September 1957 through August 1962 [Basler, 1963]. Note that the horizontal axis shows the local time, not magnetic local time. The local time at the station is approximately 2 h 40 min ahead of MLT (IGRF 1964).

and manual data sets is clearer after 2007.

The diurnal variation of ionospheric absorption has been studied by e.g. Basler [1963]. He studied the diurnal variation separately during summer, winter and equinoxes during a 5-year period (1957-1962). Figure 6.3 shows the average auroral absorption during the different seasons. He used data from College station riometer (27.6 MHz) in Alaska (geomagnetic 64.65°N, 256.56°E, L=5.5). He found that during winter months and equinoxes there appeared a broad maximum in absorption between 06-13 and minimum between 19 and 22 local time. In summer there is almost no daily variation. The average absorption during summer is also smaller than during the rest of the year. Basler's results of the diurnal variation of absorption during winter and equinoxes greatly resemble our MLT distributions.

Also the diurnal variation in figure 3.5 by Kavanagh et al. [2004], shows similar features to our results. The L-value for Kilpisjärvi (L=5.9) is not very far from e.g. Abisko (L=5.6), so their results should be similar. The average absorption has a similar distribution as most of the MLT distributions. Of course, during one year the Bz field will go through many different values and in our study we concentrated on the total amount of incidences per an hour, and not the average absorption. Still, the similarity of the distribution of the mean absorption to our MLT distributions

is not likely to be purely a coincidence and thus gives credibility to our results.

Chapter 7

Conclusions

In this project I determined a simple method for finding absorption events from riometer data. The great amount of data from the seven stations gives the results statistical reliability. However, the quality of the data is not reliable all the time. The method for determining the quiet-day curve (QDC) can have a huge effect on the quality of absorption data. We compared results received from two data sets which were based on automatic and manual QDC determination. We discovered interferences in the automatic data set caused by RFIs during the winter months of the solar cycle maximum years (2000-2003). I proceeded to remove the data from these periods and constructed the corrected automatic data set. We discovered that in this data set the yearly distributions of the number of absorption events resembled the K_p index and it had similar features to the manual data set. Based on this, we chose the corrected automatic data as our primary data set. However, the uncorrected automatic data set has similar distributions at some stations. The distributions of Abisko, Ivalo and Sodankylä were least affected by the corrections.

The MLT distributions have similar features as some earlier studies have found. The main features, the morning maximum and evening minimum, are present during most years in both automatic data set as well as the manual data. The locations of the maxima and minima change a bit during the years, but not dramatically. The MLT distributions of the stations which have nearly the same L-values are very similar during each year, especially in Abisko and Ivalo. The least absorption events are seen in 2009, which is the minimum year of the K_p index. Also the MLT distribution in 2009 is slightly different from the other years, because the morning maximum and evening minimum are not clearly visible. The biggest difference between the automatic data sets is seen during the years 2000-2003. The strong day time RFI distorts the distribution creating a broad midday maximum in the uncorrected data. During the other years the MLT distributions in the corrected and uncorrected data

sets are similar.

Many different studies can be made with the data from the SGO riometer network. The measurements of over 17 years cover more than one solar cycle, making it possible to study the variation in absorption over a long period. The locations of the seven stations make it possible to also study the latitudinal dependence. Besides the yearly and MLT distributions, the seasonal variation could be studied once the data has been verified. Also the relation between the absorption and geophysical indices could be studied more.

The interferences and problems with QDC need to be identified and somehow accounted for before we are able to publish any results. In the future the automatic QDC method should be improved, so that it doesn't take into account data during times when the riometer is saturated when calculating the quiet-day curve. Our goal is to continue this project and have results published in the near future.

Bibliography

Agy, Vaughn. The location of the auroral absorption zone. *Journal of Geophysical Research*, 59(2):267–272, 1954. ISSN 2156-2202. doi: 10.1029/JZ059i002p00267. URL http://dx.doi.org/10.1029/JZ059i002p00267.

Aikio, A. and Nygrén, T. Ionospheric physics, 2016. URL https://wiki.oulu.fi/display/~aaikio/Anita+Aikio. 76158S Ionospheric Physics, Lecture notes, University of Oulu, Last accessed 12.2.2016.

Appleton, E. V.; Naismith, R., and Builder, G. Ionospheric investigations in high latitudes. *Nature*, 132:340–341, 1933. doi: 10.1038/132340a0.

Bailey, D. K. Disturbances in the lower ionosphere observed at vhf following the solar flare of 23 february 1956 with particular reference to auroral-zone absorption. *Journal of Geophysical Research*, 62(3):431–463, 1957. ISSN 2156-2202. doi: 10.1029/JZ062i003p00431. URL http://dx.doi.org/10.1029/JZ062i003p00431.

Basler, Roy P. Radio wave absorption in the auroral ionosphere. *Journal of Geophysical Research*, 68(16):4665–4681, 1963. ISSN 2156-2202. doi: 10.1029/JZ068i016p04665. URL http://dx.doi.org/10.1029/JZ068i016p04665.

Collins, C.; Jelly, D. H., and Matthews, A. G. High-frequency radio-wave black-outs at medium and high latitudes during a solar cycle. *Canadian Journal of Physics*, 39(1):35–52, 1961. doi: 10.1139/p61-004. URL http://dx.doi.org/10.1139/p61-004.

Gosling, J. T.; Asbridge, J. R.; Bame, S. J., and Feldman, W. C. Solar wind speed variations: 19621974. *Journal of Geophysical Research*, 81(28):5061–5070, 1976. ISSN 2156-2202. doi: 10.1029/JA081i028p05061. URL http://dx.doi.org/10.1029/JA081i028p05061.

Hargreaves, J. K. Seasonal variations in the incidence of auroral radio absorption events at very high latitude, and the influence of the magnetotail. *Annales Geophysicae*, 25(3):711–720, 2007. doi: 10.5194/angeo-25-711-2007. URL http://www.ann-geophys.net/25/711/2007/.

Hargreaves, J.K. Auroral absorption of hf radio waves in the ionosphere: A review of results from the first decade of riometry. *Proceedings of the IEEE*, 57(8):1348–1373, Aug 1969. ISSN 0018-9219. doi: 10.1109/PROC.1969.7275.

Hargreaves, J.K. *The solar-terrestrial environment: an introduction to geospace – the science of the terrestrial upper atmosphere, ionosphere and magnetosphere.* Cambridge University Press, 1992.

Hargreaves, J.K. and Cowley, F.C. Studies of auroral radio absorption events at three magnetic latitudes i: Occurrence and statistical properties of the events. *Planetary and Space Science*, 15(10):1571 – 1583, 1967. ISSN 0032-0633. doi: http://dx.doi.org/10.1016/0032-0633(67)90090-6. URL http://www.sciencedirect.com/science/article/pii/0032063367900906.

Hargreaves, J.K.; Feeney, M.T.; Ranta, H., and Ranta, A. On the prediction of auroral radio absorption on the equatorial side of the absorption zone. *Journal of Atmospheric and Terrestrial Physics*, 49(3):259 – 272, 1987. ISSN 0021-9169. doi: http://dx.doi.org/10.1016/0021-9169(87)90061-4. URL http://www.sciencedirect.com/science/article/pii/0021916987900614.

Hartz, T. R.; Montbriand, L. E., and Vogan, E. L. A study of auroral absorption at 30mc/s. *Canadian Journal of Physics*, 41(4):581–595, 1963. doi: 10.1139/p63-061. URL http://dx.doi.org/10.1139/p63-061.

Heppner, J. P.; Byrne, E. C., and Belon, A. E. The association of absorption and es ionization with aurora at high latitudes. *Journal of Geophysical Research*, 57(1):121–134, 1952. ISSN 2156-2202. doi: 10.1029/JZ057i001p00121. URL http://dx.doi.org/10.1029/JZ057i001p00121.

Hunsucker, R.D. and Hargreaves, J.K. *The high-latitude ionosphere and its effects on radio propagation.* Cambridge University Press, 2003.

INGV, . Electron density profiles, 2015. URL http://roma2.rm.ingv.it/en/research_areas/4/ionosphere. Retrieved 29.11.2015.

IRIS, . Iris-imaging riometer for ionospheric studies, 2015. URL http://spears.lancs.ac.uk/iris/. Lancaster University, Retrieved 6.3.2016.

Kavanagh, A. J. *Energy deposition in the lower auroral ionosphere through energetic particle precipitation.* PhD thesis, Department of Communication Systems, Lancaster University, UK, 2002.

Kavanagh, A. J.; Kosch, M. J.; Honary, F.; Senior, A.; Marple, S. R.; Woodfield, E. E., and McCrea, I. W. The statistical dependence of auroral absorption on geomagnetic and solar wind parameters. *Annales Geophysicae*, 22(3):877–887, 2004. doi: 10.5194/angeo-22-877-2004. URL `http://www.ann-geophys.net/22/877/2004/`.

LaJolla, . Riometer block diagram, 2010. URL `http://www.lajollasciences.com/block.html`. Retrieved 10.9.2015.

Little, C.G. and Leinbach, H. The riometer-a device for the continuous measurement of ionospheric absorption. *Proceedings of the IRE*, 47(2):315–320, Feb 1959. ISSN 0096-8390. doi: 10.1109/JRPROC.1959.287299.

McIlwain, Carl E. Coordinates for mapping the distribution of magnetically trapped particles. *Journal of Geophysical Research*, 66(11):3681–3691, 1961. ISSN 2156-2202. doi: 10.1029/JZ066i011p03681. URL `http://dx.doi.org/10.1029/JZ066i011p03681`.

McKay-Bukowski, D.; Vierinen, J.; Virtanen, I. I.; Fallows, R.; Postila, M.; Ulich, T.; Wucknitz, O.; Brentjens, M.; Ebbendorf, N.; Enell, C. F.; Gerbers, M.; Grit, T.; Gruppen, P.; Kero, A.; Iinatti, T.; Lehtinen, M.; Meulman, H.; Norden, M.; Orispää, M.; Raita, T.; de Reijer, J. P.; Roininen, L.; Schoenmakers, A.; Stuurwold, K., and Turunen, E. Kaira: The kilpisjärvi atmospheric imaging receiver array;system overview and first results. *IEEE Transactions on Geoscience and Remote Sensing*, 53(3):1440–1451, March 2015. ISSN 0196-2892. doi: 10.1109/TGRS.2014.2342252.

Mursula, K. Basics of space physics, 2015. URL `https://wiki.oulu.fi/display/766355A/Etusivu`. 766355A Basics of Space Physics, Lecture notes, University of Oulu, Last accessed 15.2.2016.

Mursula, K. Heliospheric physics, 2016. URL `https://wiki.oulu.fi/display/766656S`. 766656S Heliospheric Physics, Lecture notes, University of Oulu, Last accessed 1.2.2016.

NASA, . Earth's magnetosphere, 2007. URL `http://science.nasa.gov/newhome/headlines/guntersville98/images/mag_sketch_633.jpg`. National Aeronautics and Space Administration, Retrieved 20.10.2015.

Obayashi, Tatsuzo and Hakura, Yukio. Solar corpuscular radiation and polar ionospheric disturbances. *Journal of Geophysical Research*, 65(10):3131–3142, 1960.

ISSN 2156-2202. doi: 10.1029/JZ065i010p03131. URL http://dx.doi.org/10.1029/JZ065i010p03131.

Ortner, J.; Hultqvist, B.; Brown, R. R.; Hartz, T. R.; Holt, O.; Landmark, B.; Hook, J. L., and Leinbach, H. Cosmic noise absorption accompanying geomagnetic storm sudden commencements. *Journal of Geophysical Research*, 67(11):4169–4186, 1962. ISSN 2156-2202. doi: 10.1029/JZ067i011p04169. URL http://dx.doi.org/10.1029/JZ067i011p04169.

Reid, G. C. and C., Collins. Observations of abnormal vhf radio wave absorption at medium and high latitudes. *Journal of Atmospheric and Terrestrial Physics*, 1:63, 1959. doi: doi:10.1016/0021-9169(59)90056-X.

SGO, Sodankylä Geophysical Observatory. Riometer map, 2015. URL http://sgo.fi/Data/Riometer/riometer.php. Retrieved 10.9.2015.

Thorne, Richard M.; Horne, Richard B.; Glauert, Sarah; Meredith, Nigel P.; Shprits, Yuri Y.; Summers, Danny, and Anderson, Roger R. *The Influence of Wave-Particle Interactions on Relativistic Electron Dynamics During Storms*, pages 101–112. American Geophysical Union, 2013. ISBN 9781118666128. doi: 10.1029/159GM07. URL http://dx.doi.org/10.1029/159GM07.

UCAR, University Corporation for Atmospheric Research. Ballerina skirt model of the heliomagnetic current sheet, 2000. URL http://www.windows2universe.org/spaceweather/ballerina_skirt.html. Retrieved 20.10.2015.

Wells, H. W. Polar radio disturbances during magnetic bays. *Terrestrial Magnetism and Atmospheric Electricity*, 52(3):315–320, 1947. ISSN 0096-8013. doi: 10.1029/TE052i003p00315. URL http://dx.doi.org/10.1029/TE052i003p00315.

Zolesi, B. and Cander, L.R. *Ionospheric Prediction and Forecasting*. Springer Geophysics. Springer Berlin Heidelberg, 2013. ISBN 9783642384301. URL https://books.google.fi/books?id=bj65BAAAQBAJ.

Appendices

Appendix A

Uncorrected automatic data

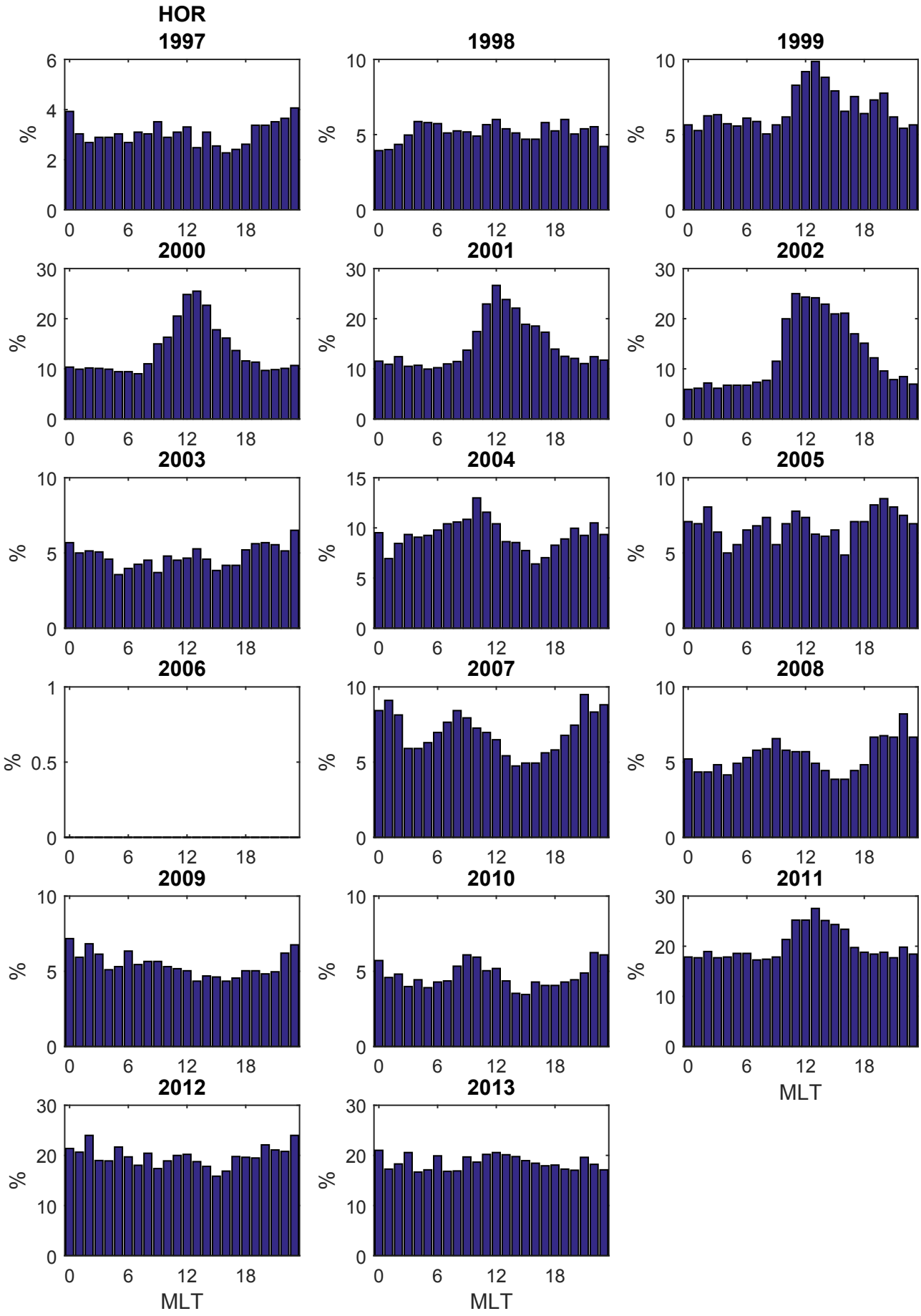
HOR
1997
1998
1999
2000
2001
2002
2003
2004
2005
2006
2007
2008
2009
2010
2011
2012
2013
%
MLT
0
6
12
18

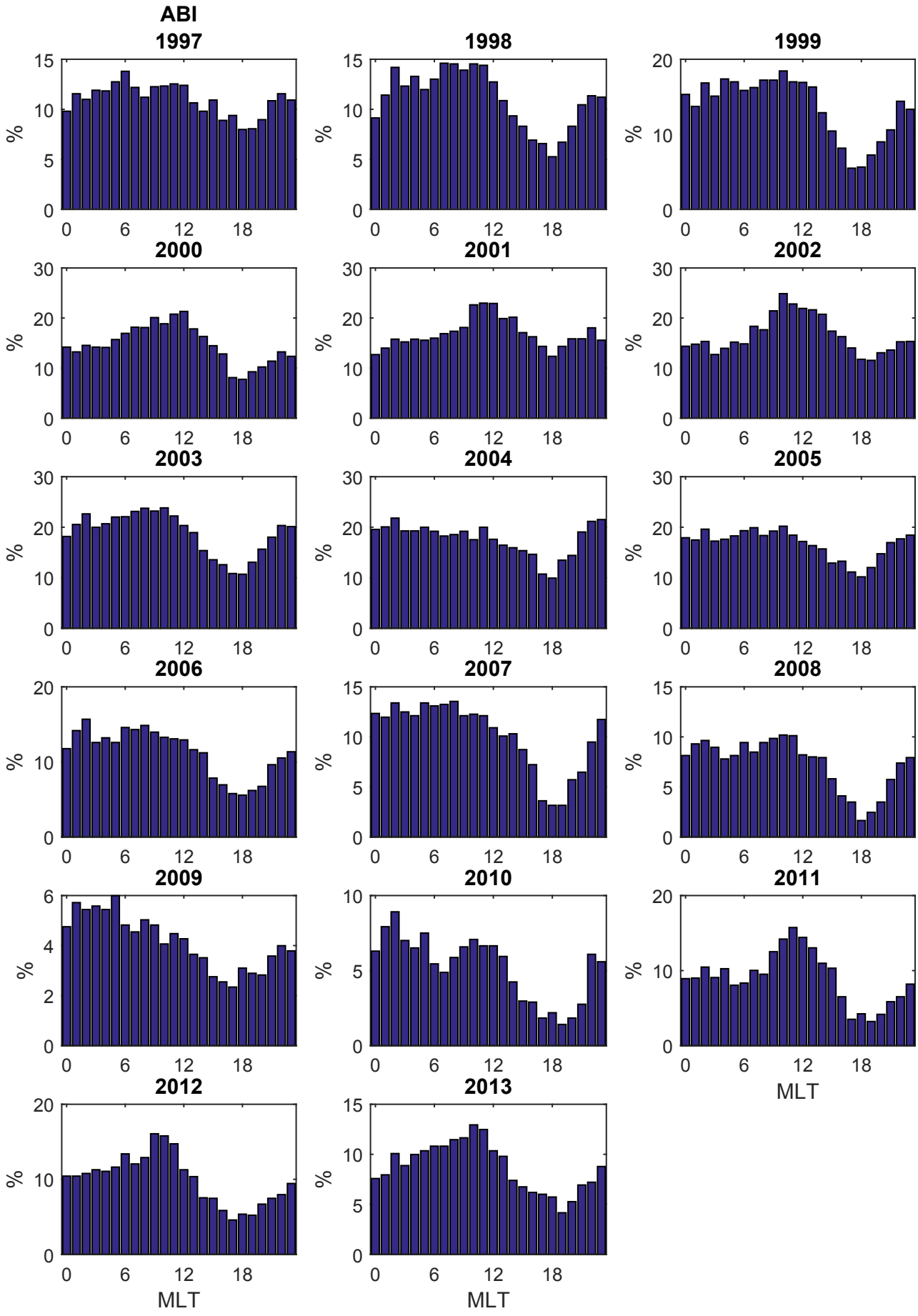
ABI
1997
1998
1999
2000
2001
2002
2003
2004
2005
2006
2007
2008
2009
2010
2011
2012
2013
%
MLT
0
6
12
18

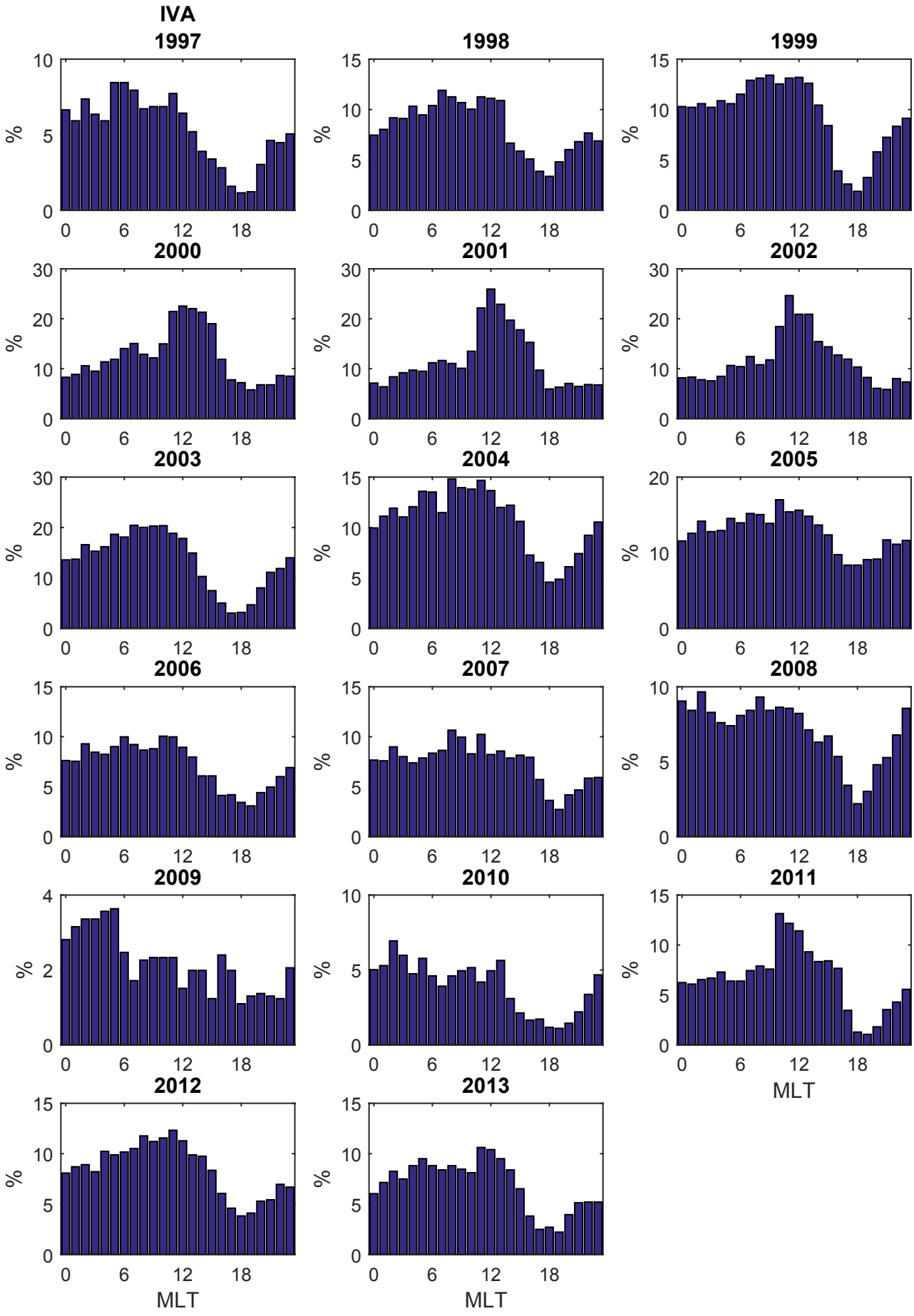
IVA
1997
1998
1999
2000
2001
2002
2003
2004
2005
2006
2007
2008
2009
2010
2011
2012
2013
%
MLT
0
6
12
18

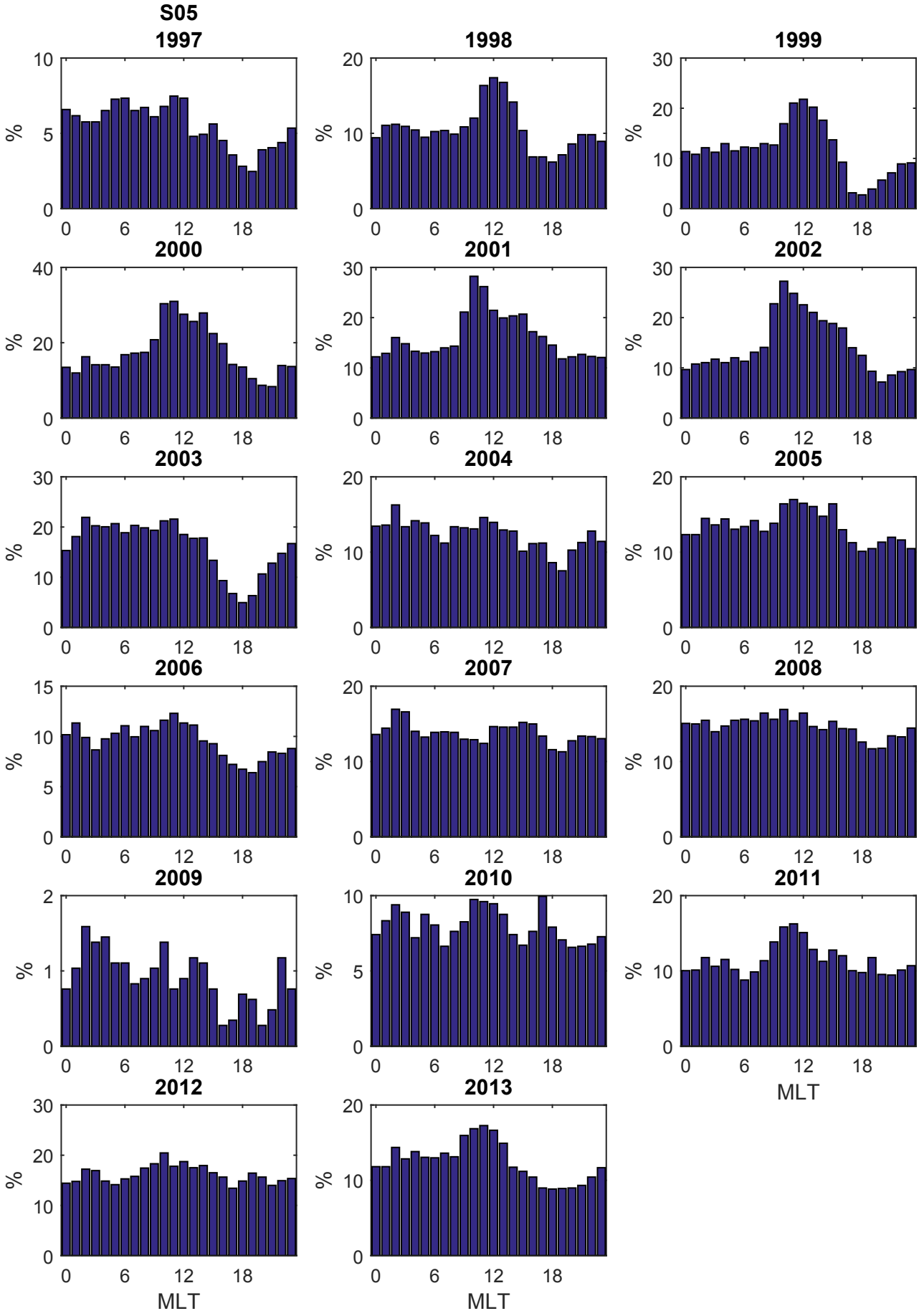
S05
1997
1998
1999
2000
2001
2002
2003
2004
2005
2006
2007
2008
2009
2010
2011
2012
2013
%
MLT
0
6
12
18

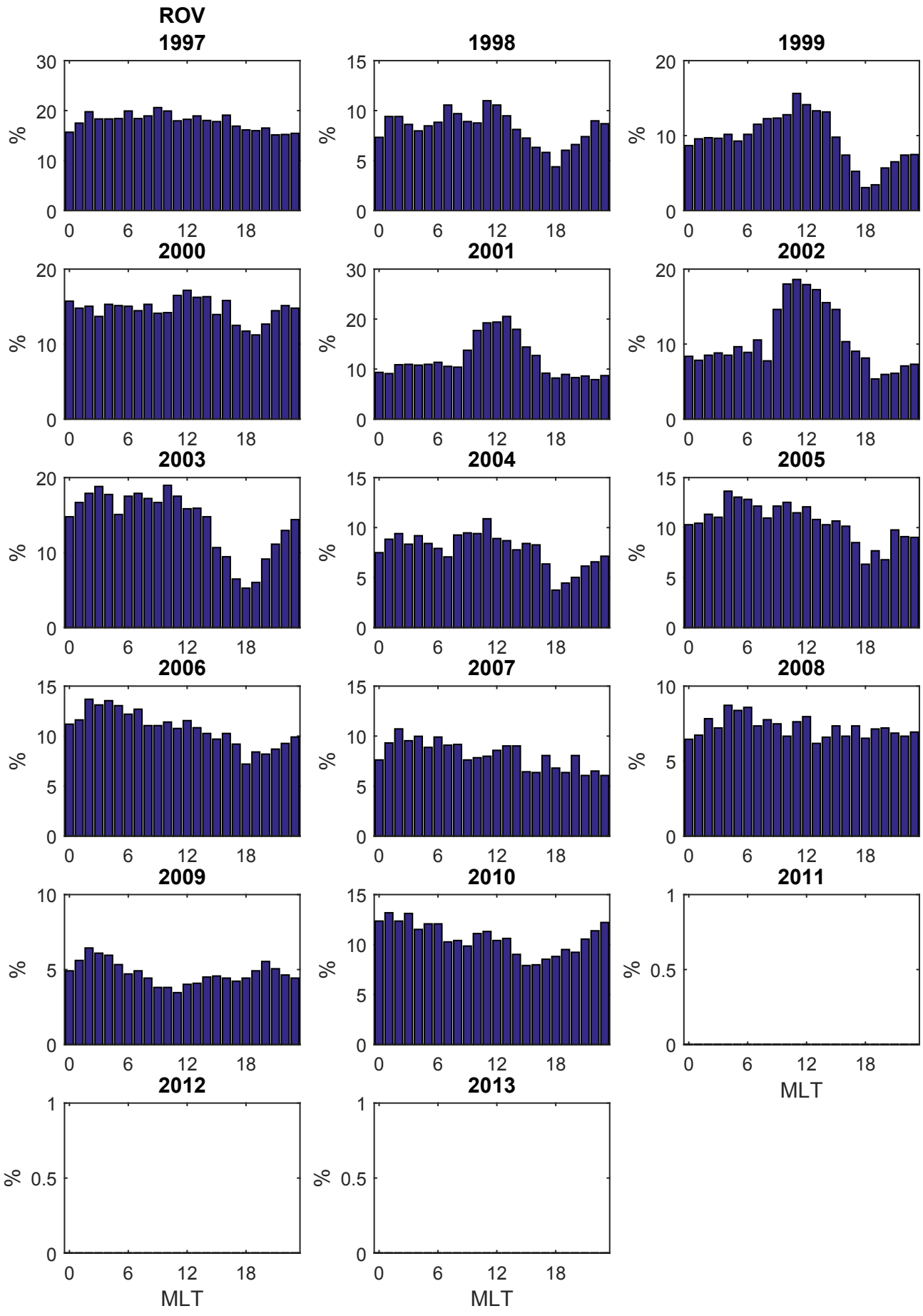
ROV
1997
1998
1999
2000
2001
2002
2003
2004
2005
2006
2007
2008
2009
2010
2011
2012
2013
%
MLT
0
6
12
18

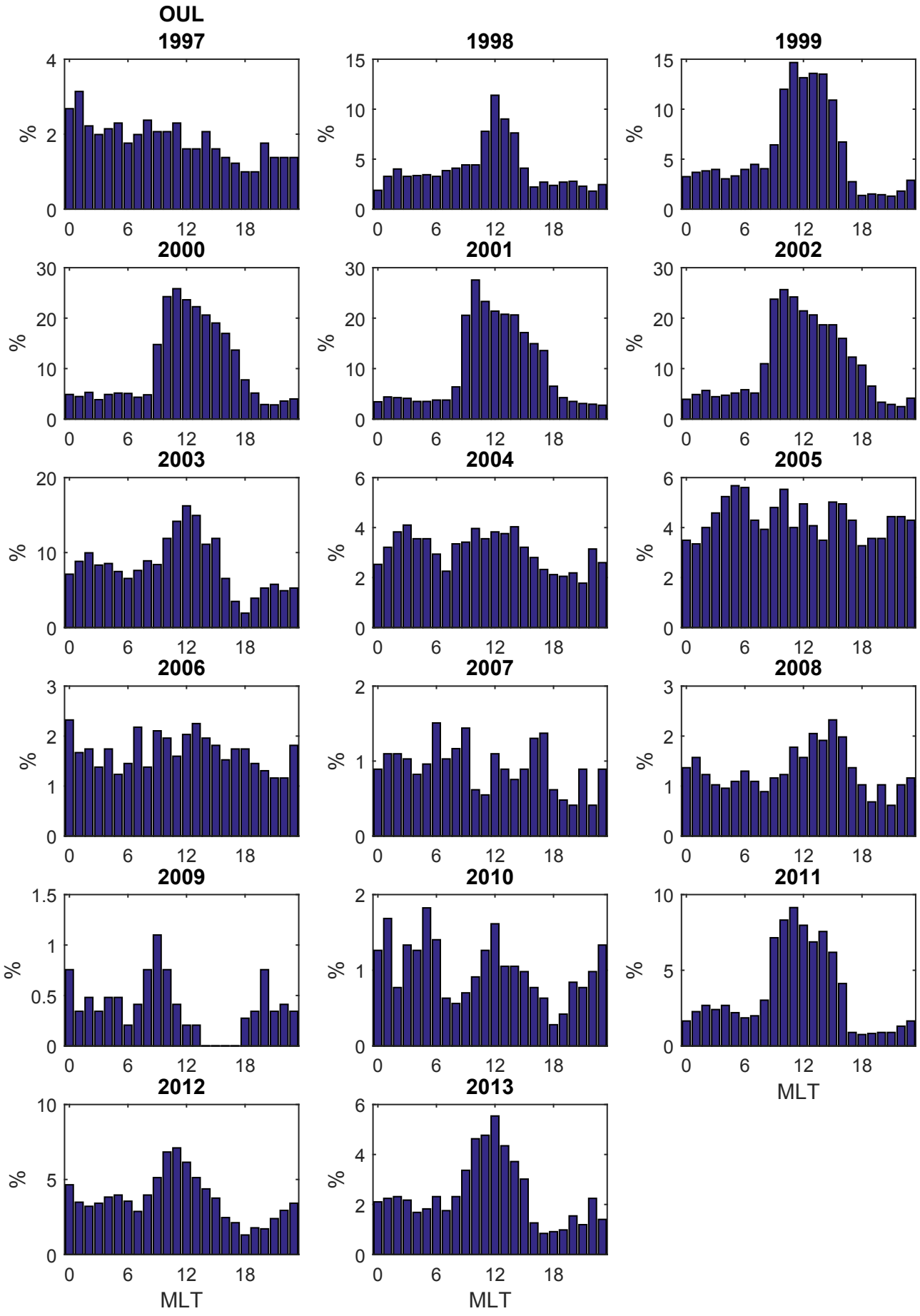
OUL
1997
1998
1999
2000
2001
2002
2003
2004
2005
2006
2007
2008
2009
2010
2011
2012
2013
%
MLT
0
6
12
18

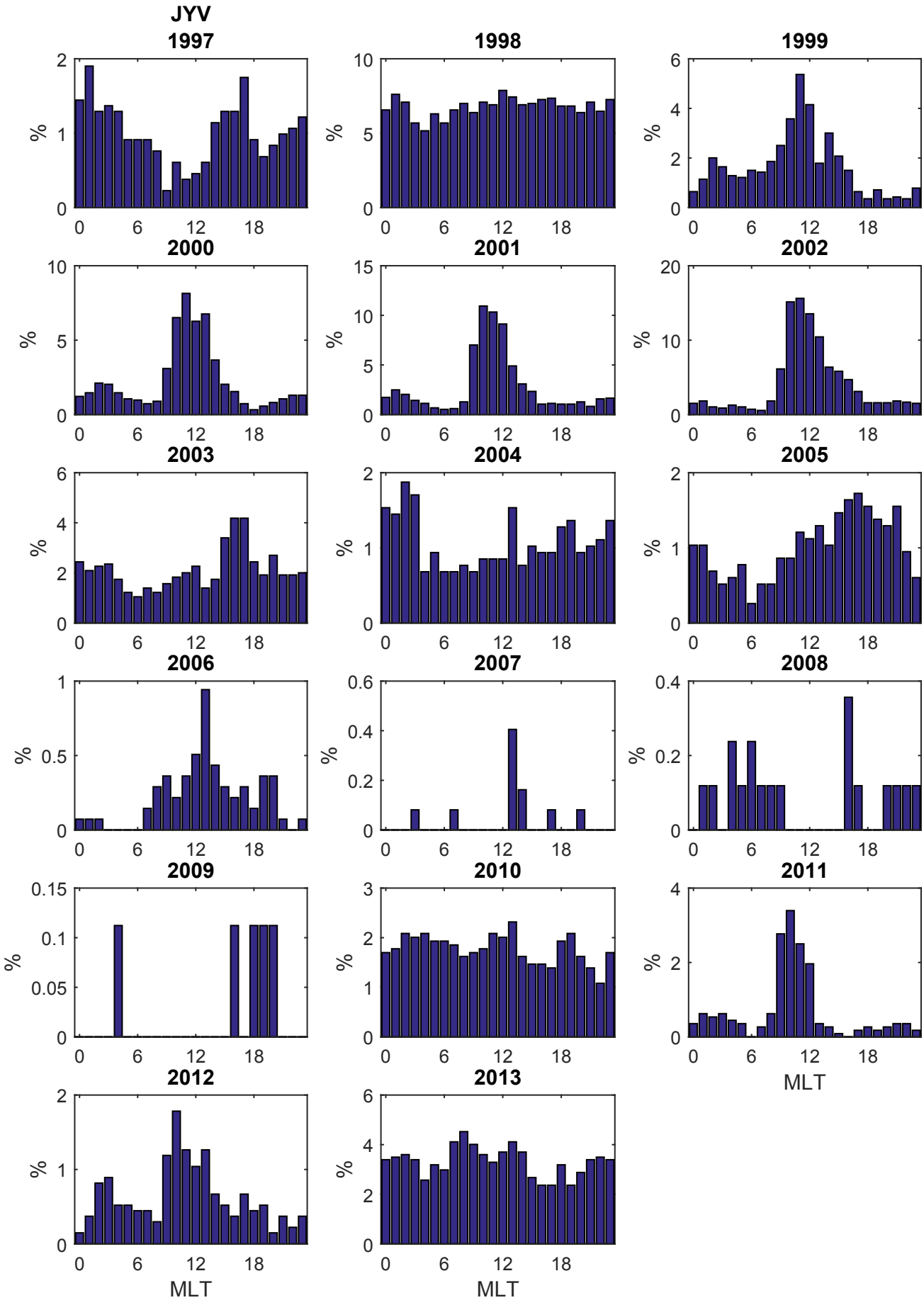
JYV
1997
1998
1999
2000
2001
2002
2003
2004
2005
2006
2007
2008
2009
2010
2011
2012
2013
%
MLT
0
6
12
18

Appendix B

Manual data

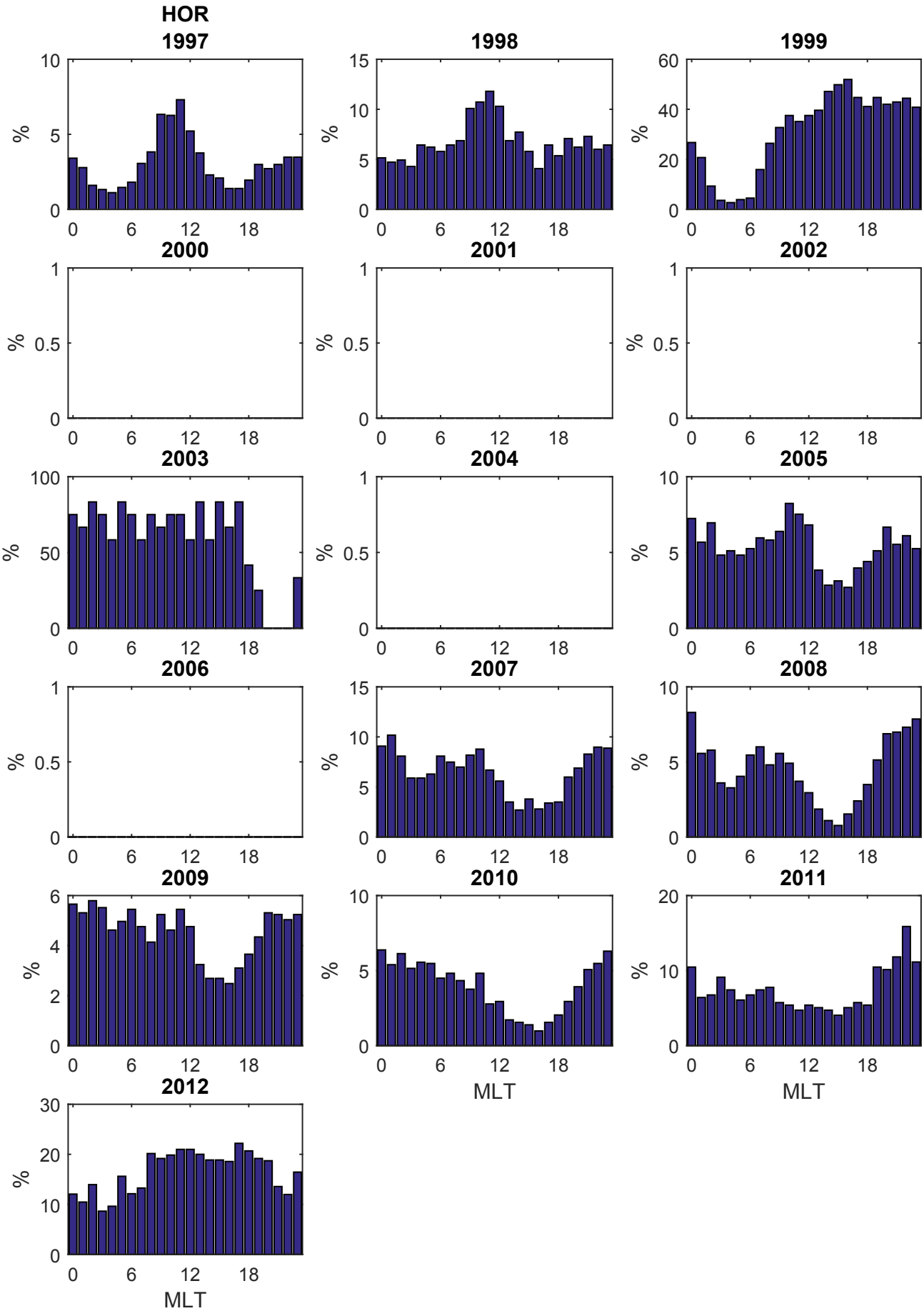
HOR
1997
1998
1999
2000
2001
2002
2003
2004
2005
2006
2007
2008
2009
2010
2011
2012
%
MLT
0
6
12
18

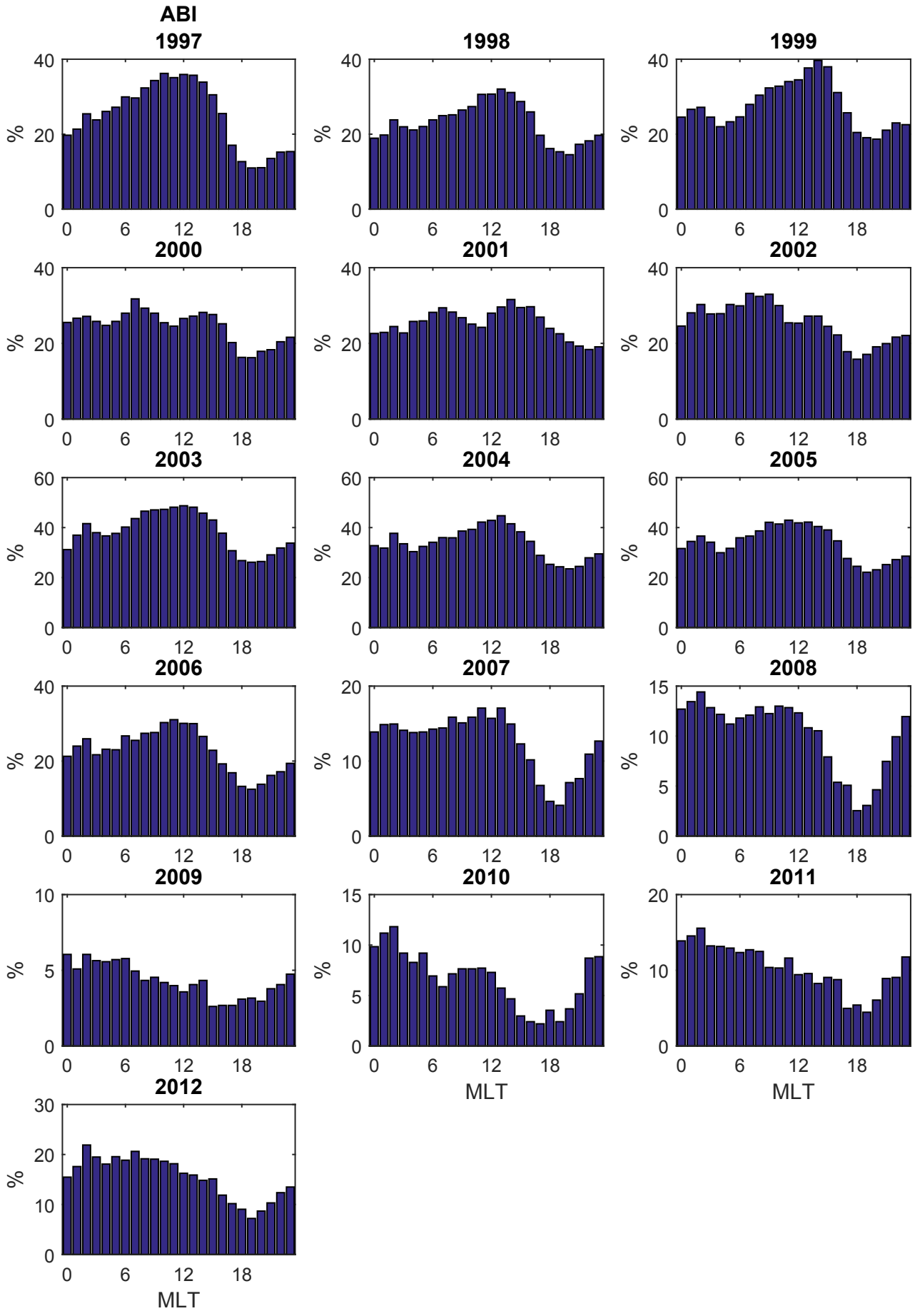
ABI
1997
1998
1999
2000
2001
2002
2003
2004
2005
2006
2007
2008
2009
2010
2011
2012
%
MLT
0
6
12
18

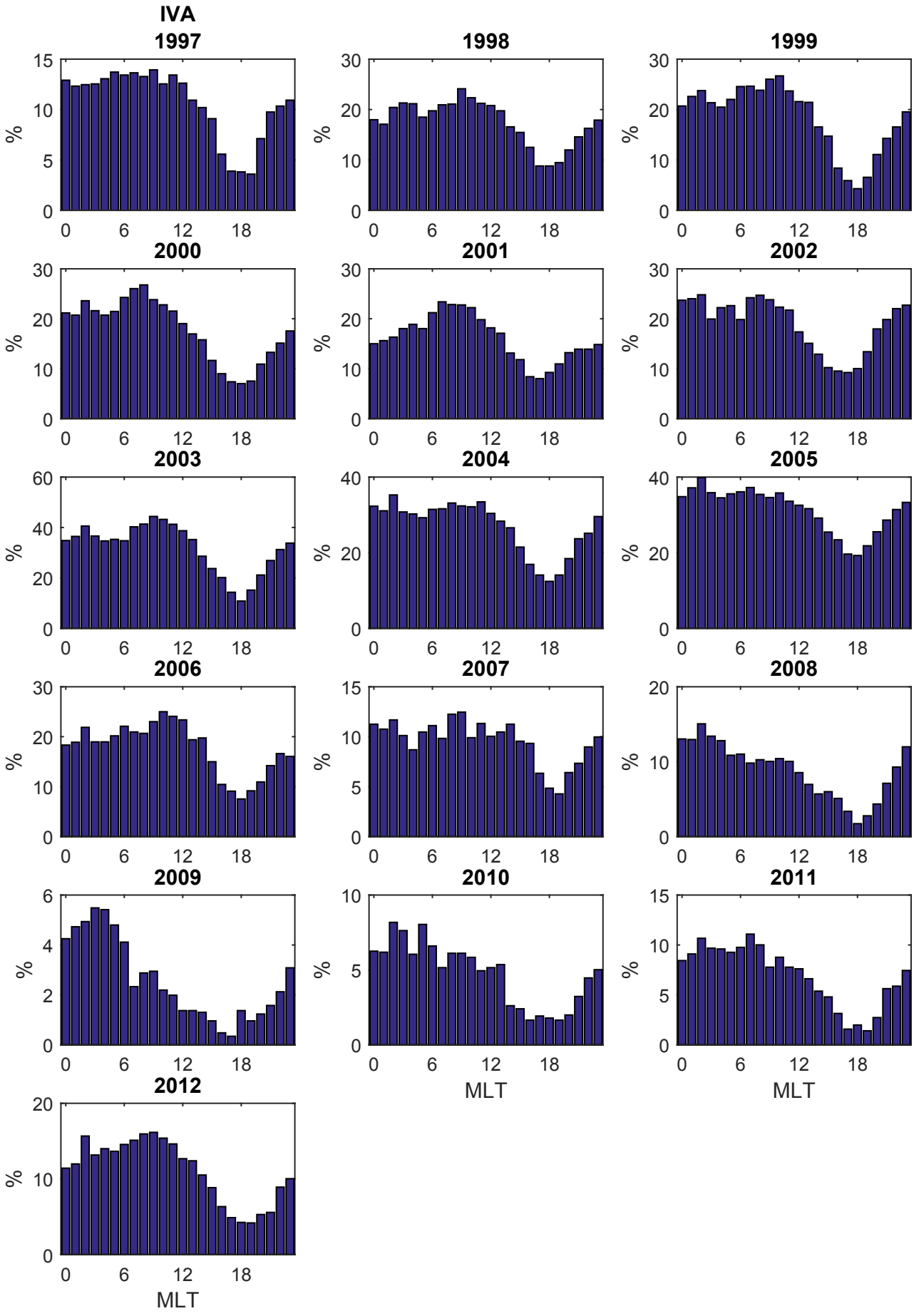
IVA
1997
1998
1999
2000
2001
2002
2003
2004
2005
2006
2007
2008
2009
2010
2011
2012
%
MLT
0
6
12
18

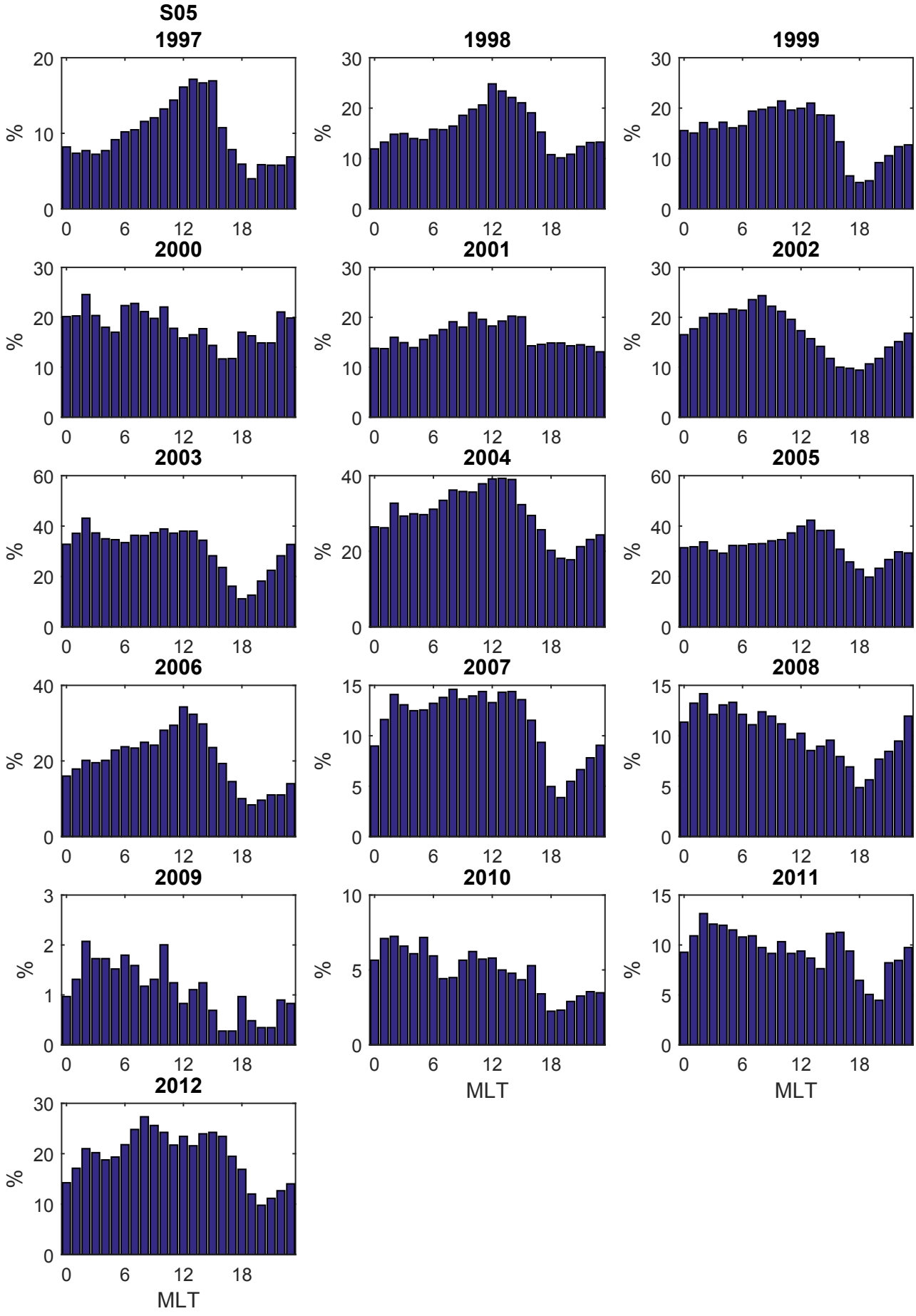
S05
1997
1998
1999
2000
2001
2002
2003
2004
2005
2006
2007
2008
2009
2010
2011
2012
%
MLT
0
6
12
18

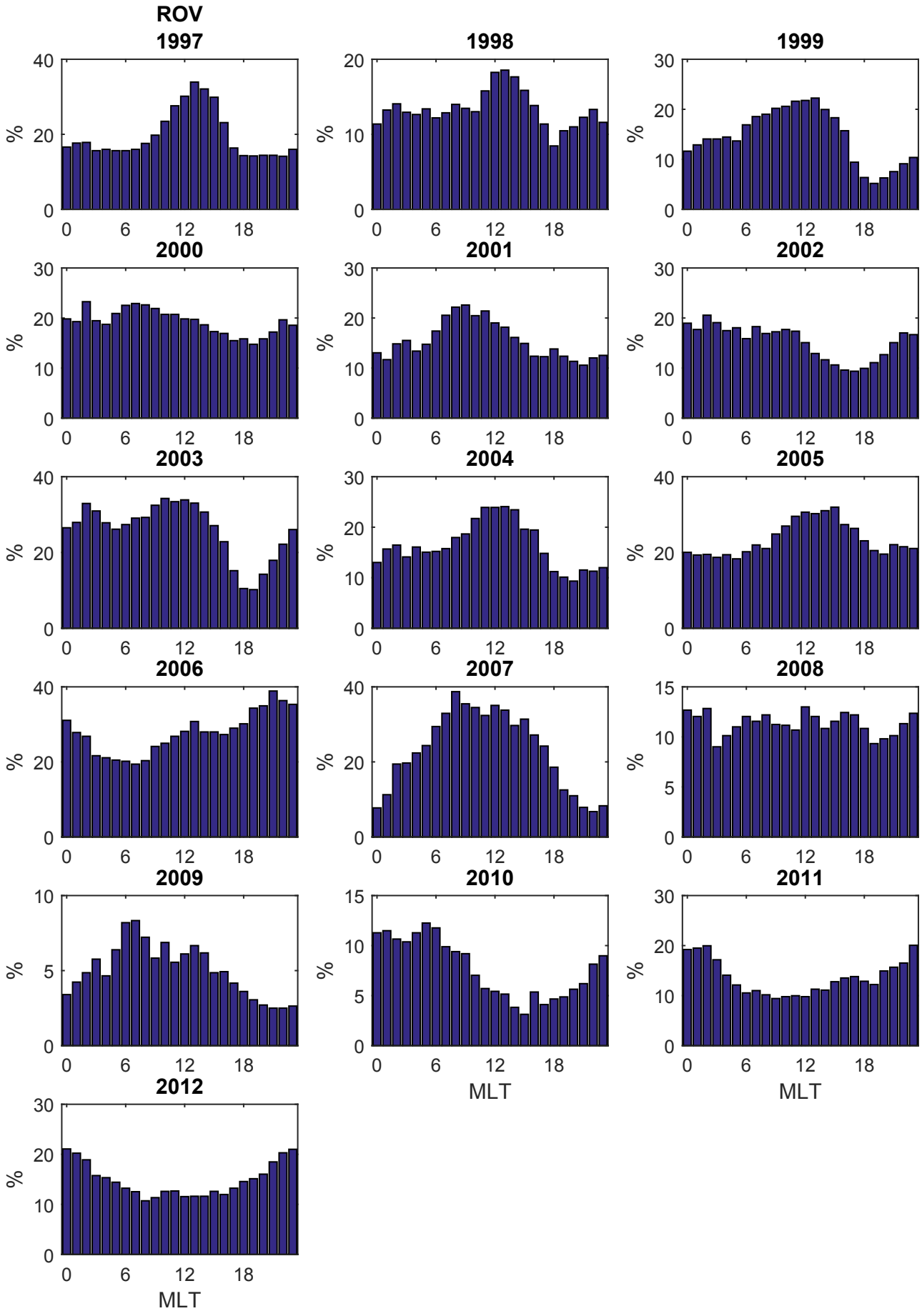
ROV
1997
1998
1999
2000
2001
2002
2003
2004
2005
2006
2007
2008
2009
2010
2011
2012
%
MLT
0
6
12
18

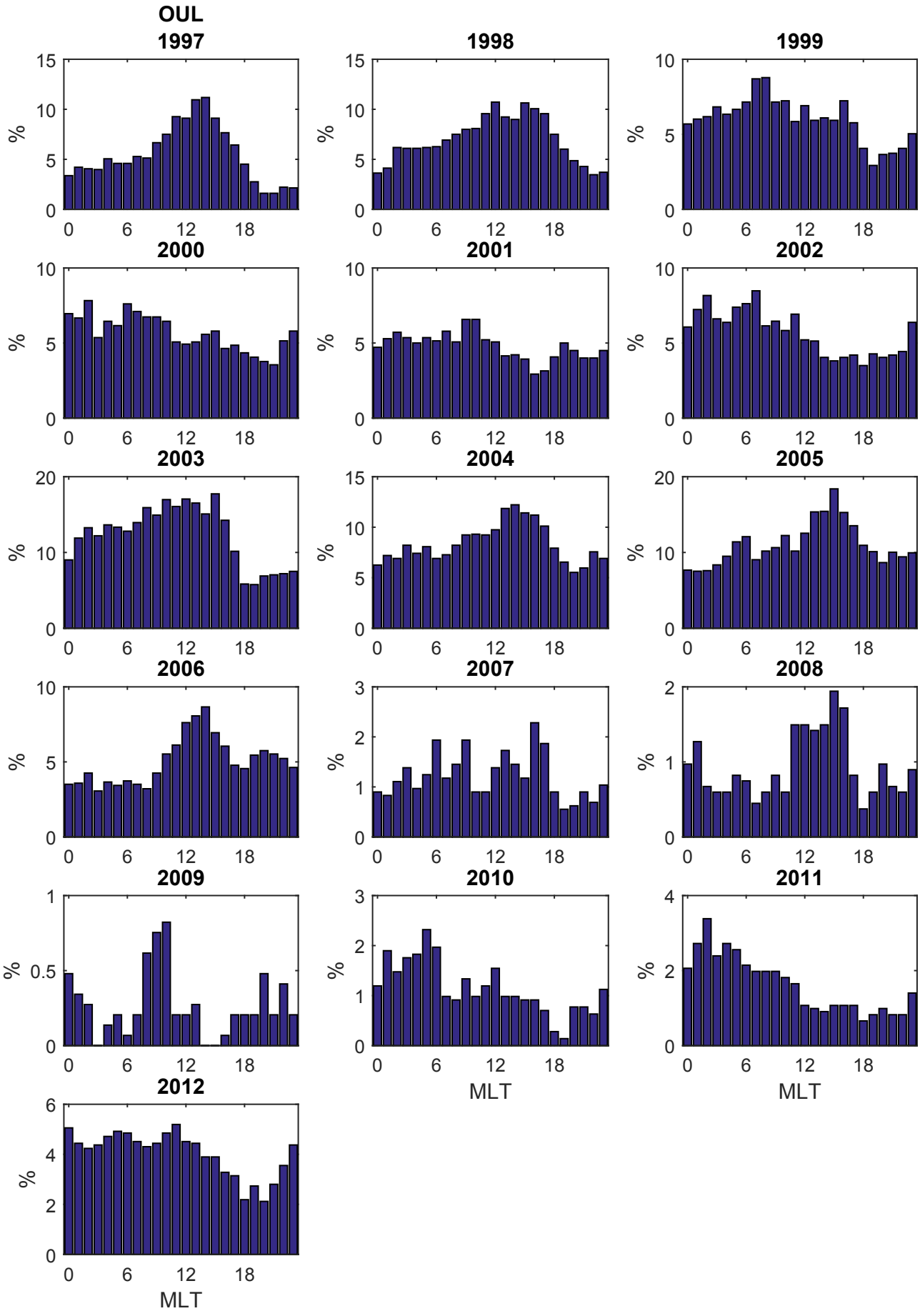
OUL
1997
1998
1999
2000
2001
2002
2003
2004
2005
2006
2007
2008
2009
2010
2011
2012
%
MLT
0
6
12
18

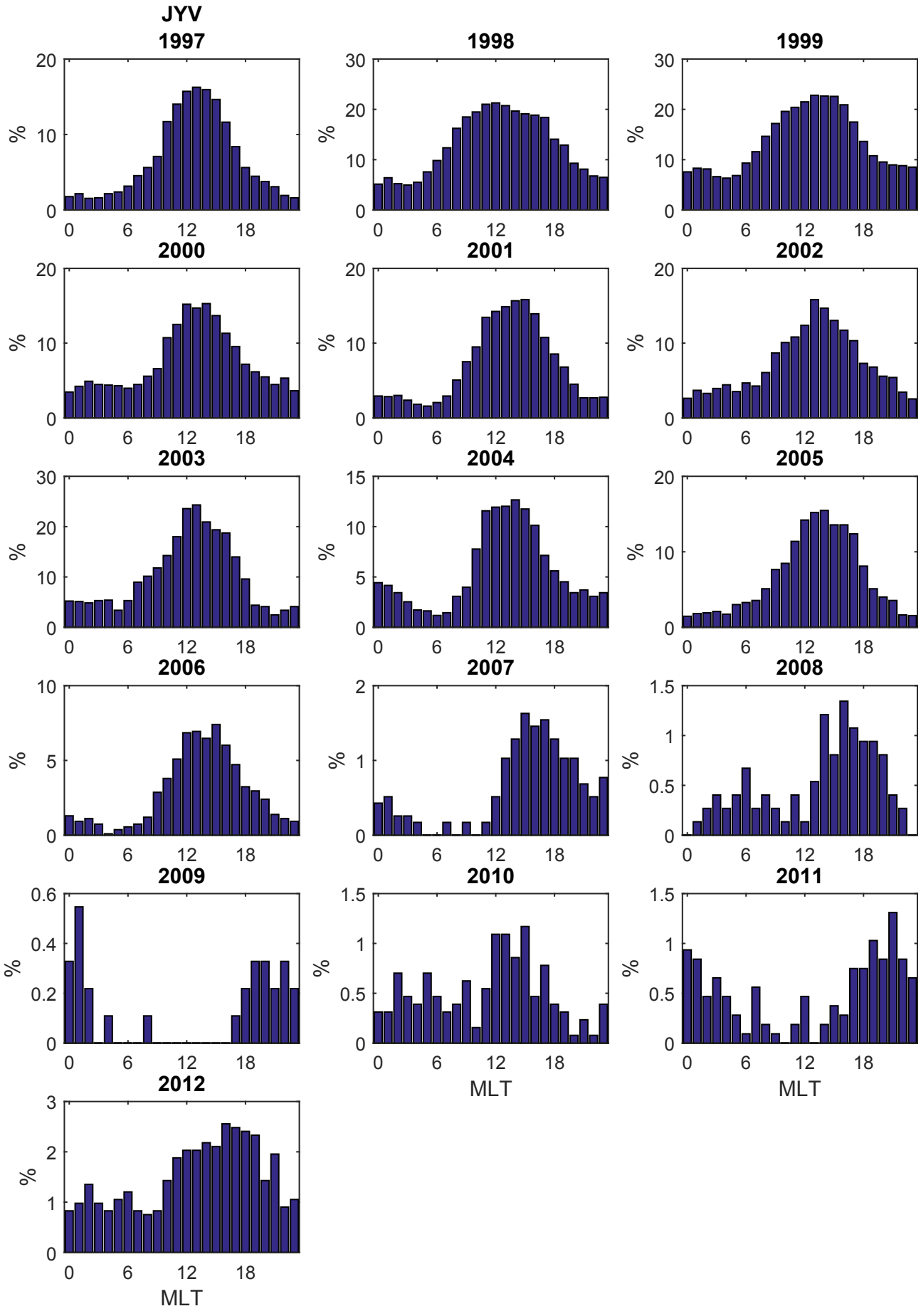
JYV
1997
1998
1999
2000
2001
2002
2003
2004
2005
2006
2007
2008
2009
2010
2011
2012
%
MLT
0
6
12
18